Reconstruction of e^+e^- in peripheral Au+Au collisions at $\sqrt{s_{NN}} = 2.42\,GeV$ with HADES

Rekonstruktion von e^+e^- in peripheren Au+Au Kollisionen bei $\sqrt{s_{NN}} = 2.42\,GeV$ mit HADES
Bachelor-Thesis von Niklas Schild aus Darmstadt
Tag der Einreichung: 31.07.2018

1. Gutachten: Prof. Dr. Tetyana Galatyuk
2. Gutachten: Dr. Szymon Harabasz

TECHNISCHE
UNIVERSITÄT
DARMSTADT

Fachbereich Physik
Institut für Kernphysik

Reconstruction of e^+e^- in peripheral Au+Au collisions at $\sqrt{s_{NN}} = 2.42\ GeV$ with HADES
Rekonstruktion von e^+e^- in peripheren Au+Au Kollisionen bei $\sqrt{s_{NN}} = 2.42\ GeV$ mit HADES

Vorgelegte Bachelor-Thesis von Niklas Schild aus Darmstadt

1. Gutachten: Prof. Dr. Tetyana Galatyuk
2. Gutachten: Dr. Szymon Harabasz

Tag der Einreichung: 31.07.2018

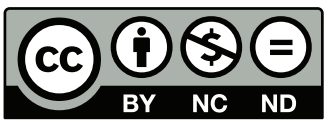

Erklärung zur Bachelor-Thesis

Hiermit versichere ich, die vorliegende Bachelor-Thesis ohne Hilfe Dritter nur mit den angegebenen Quellen und Hilfsmitteln angefertigt zu haben. Alle Stellen, die aus Quellen entnommen wurden, sind als solche kenntlich gemacht. Diese Arbeit hat in gleicher oder ähnlicher Form noch keiner Prüfungsbehörde vorgelegen.

Darmstadt, den 30. Juli 2018

(Niklas Schild)

Abstract

The investigation of hadronic matter in hot and dense conditions is a key research topic in the HADES collaboration and for many nuclear physicists around the world. To gain insight in the behaviour of strongly interacting particles, heavy ions are collided with relativistic speeds. Detection of particles created during a collision brings information about the properties of particles and eventually leads to a more detailed picture of the QCD phase diagram. e^+e^- pairs serve as a particularly interesting probe of the fireball as they do not interact strongly, but are influenced overwhelmingly by the electromagnetic force. Once created, through one of their many sources, this means that such dileptons can reach the detector directly and unhindered, such that they bring information about the early stages of the collision. Using the experimental data from 2012 Au+Au collisions at $\sqrt{s} = 2.42\ GeV$ at HADES, these dileptons are identified and their invariant mass spectrum investigated. A particular focus is set on the inspection of peripheral events which have largely been ignored in previous works due to their limited statistics. This analysis includes an event selection, a single lepton identification and a subsequent signal extraction for which the combinatorial background is calculated. Furthermore, the signal is acceptance and efficiency corrected. On top of that, a normalisation to the number of π^0 is applied and the excess pairs are isolated by subtracting reference and η-spectrum. This allows to calculate the excess yield and temperature from the remaining invariant mass spectra and their behaviour as a function of the mean number of participating nucleons A_{part} is investigated.

Zusammenfassung

Die Untersuchung von hadronischer Materie unter heißen und dichten Bedingungen ist ein zentrales Forschungsthema in der HADES Kollaboration und von vielen Physiker in der ganzen Welt. Um Einsicht in das Verhalten von stark wechselwirkenden Teilchen zu erhalten, werden schwere Ionen mit relativistischen Geschwindigkeiten kollidiert. Die Detektion der in der Kollision entstehenden Teilchen liefert Informationen über die Eigenschaften der Teilchen und führt schließlich zu einem detaillierten Bild des QCD-Phasendiagramms. e^+e^- Paare agieren als besonders interessante Probe des Feuerballs, da sie nicht stark wechselwirken, sondern überwiegend von der elektromagnetischen Kraft beeinflusst sind. Wenn sie einmal durch eine ihrer vielen Quellen entstanden sind, bedeutet dies, dass jene Dileptonen den Detektor direkt und unbehindert erreichen können und somit Informationen über die frühen Phasen der Kollision bringen. Unter der Nutzung der experimentellen Daten von Au+Au Kollisionen aus dem Jahr 2012 bei $\sqrt{s} = 2.42\ GeV$ (gemessen bei HADES) werden Dileptonen identifiziert und deren invariantes Massenspektrum untersucht. Ein besonderer Fokus wird auf die Inspektion von peripheren Kollisionsereignissen gesetzt, welche in vorherigen Arbeiten aufgrund ihrer limitierten Statistik größtenteils ignoriert wurden. Diese Analyse beinhaltet eine Selektion von Kollisionsereignissen, eine Leptonenidentifikation und die anschließende Extraktion des Signals, wobei dafür der kombinatorielle Hintergrund berechnet wird. Weiterhin wird das Signal um die Akzeptanz und Effizienz korrigiert. Darüberhinaus wird eine Normalisierung zu der Anzahl der π^0 durchgeführt und die überschüssigen Paare werden isoliert, indem die Referenz und das η-Spectrum abgezogen werden. Das ermöglicht die Berechnung der überschüssigen Ausbeute und Temperatur aus den übrig gebliebenen invarianten Massenspektren und deren Verhalten als Funktion von der durchschnittlichen Anzahl von teilnehmenden Nukleonen A_{part} wird untersucht.

Contents

List of Figures

List of Tables

1 Introduction

1.1 Standard model and quantum chromodynamics

One of todays most important and widely applied theory on the inner workings of the universe is the standard model. It is believed that all matter is made up of a handful of fundamental particles that can be divided into fermions with half-integer spin and bosons with integer spin. Bosons, on the one hand, act as force carriers, namely photons carry the electromagnetic, gluons the strong and W or Z bosons the weak interactions. The gravitational force is not described with the standard model. Fermions, on the other hand, generally act as the matter particles. As shown in figure 1.1 they are furthermore separated into quarks and leptons depending on their color charge. Leptons lack color charge and, in contrast to quarks, do not feel the strong interaction.

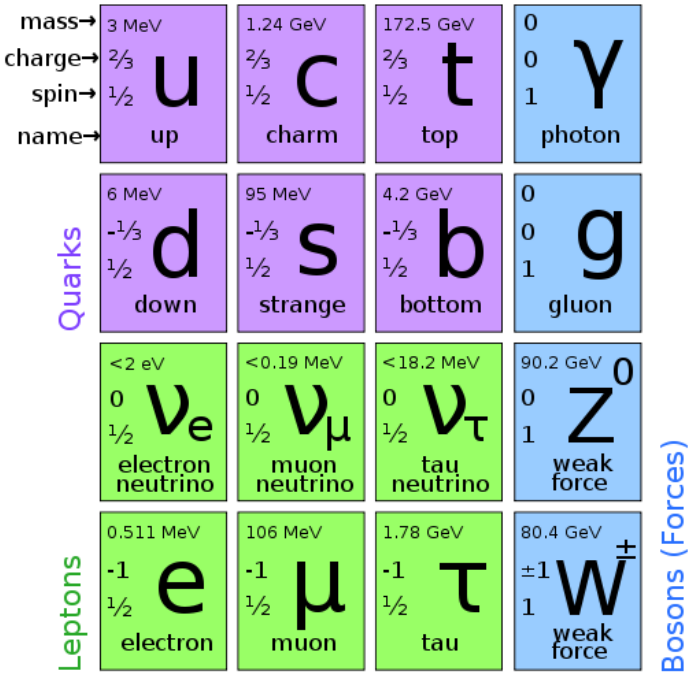

Figure 1.1: Standard Model - Fundamental particles and their basic properties. Figure from: `http://www.newworldencyclopedia.org/entry/File:Standard_Model_of_Elementary_Particles.svg` (accessed 23.05.16)

In the standard model the strong interaction is described by quantum chromodynamics (QCD). One of its most essential assertions is the principle of confinement which is the phenomenon that particles with color charge, namely quarks or gluons, cannot be encountered isolated but instead always confine with other quarks/gluons or antiquarks/antigluons to appear with total color charge zero. Hence, in ordinary conditions quarks confine to colorless hadrons which can only interact strongly on short distances ($\sim$ fm) via the residual strong force.

However, in extreme conditions the properties of hadronic matter seem to change. It is believed that given sufficient temperature T or density ρ nuclear matter can reach different phases, in particluar a state of Quark-Gluon Plasma (QGP). In such a plasma hadrons overlap

and quarks from different hadrons interact directly and with such frequency that a distinction between hadrons can no longer be made. The investigation of such conditions is of considerable interest for physics research today. A better understanding of the strong force and the behaviour of strongly interacting particles is one of the goals pursued at particle accelerators worldwide.

The ultimate goal would be to draw a phase diagram as a function of temperature T and density ρ which illustrates how and when different states of matter are reached. Alternatively one can draw a phase diagram as function of the baryon chemical potential μ_B, as it is directly related to the density ρ. The exact location of phase boundaries and the nature of the phase transitions as well as the possibility of a critical point remain a topic for discussion at this point and are based mainly on Lattice QCD inspired theories.

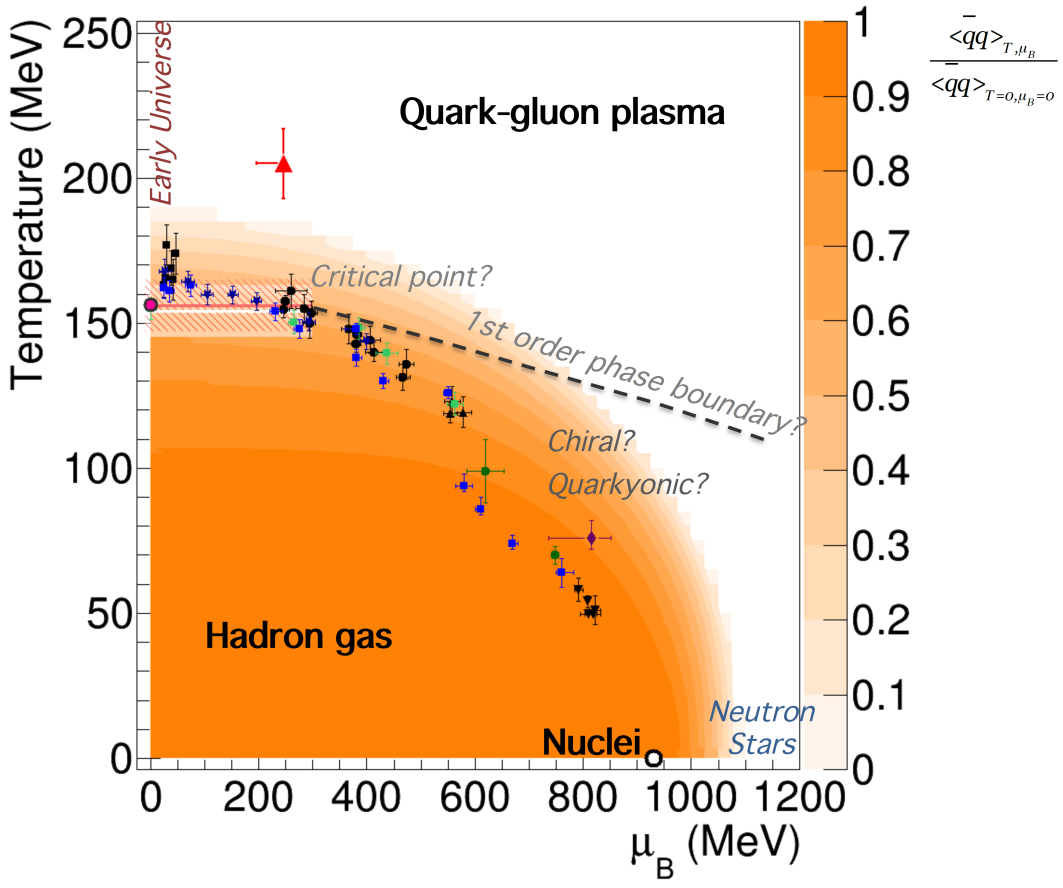

Figure 1.2: QCD Phase diagram. The data points indicate freeze out conditions at different experiments as calculated using thermal models. They differentiate in their beam energies with one the one side, LHC energies of few TeV/u producing high temperatures at low densities and one the other side, SIS energies of a few GeV/u producing lower temperatures but at higher densities. In the z-Axis one can see a possible calculation for the chiral condensate which is explained further below. Figure from [18].

The data from this work stems from the SIS18 accelerator at GSI, Darmstadt. From the figure above it can be seen that no Quark-Gluon Plasma is expected to be reached at these energies. However even approaching the more extreme conditions brings information about the phase diagram. This is indicated in the z-Axis in Figure 1.2 which shows shows the expectation

value of the chiral condensate. One of the ways it can be calculated is using the low density approximation [19]:

$$\frac{\langle\langle\bar{q}q\rangle\langle(T,\mu_B)}{\langle\bar{q}q\rangle} \approx 1 - \frac{T^2}{8f_\pi^2} - \frac{\rho_N}{3\rho_0} \tag{1.1}$$

This shows another important effect that occurs when the system moves away from ordinary conditions. In ordinary conditions (vacuum) the so-called chiral symmetry is spontaneously broken. The chiral condensate indicates how this shifts and the chiral symmetry approaches restoration for increasing temperature and density.

This effect is also visible looking at particle spectra. As shown in figure 1.3 two chiral partners have clearly separate properties at ordinary conditions. This is because chiral symmetry is broken. By increasing the temperature of the system, this effect starts to diminish to a point in which the two particles are no longer distinguishable. In this way it is possible to spectate the chiral symmetry as it approaches restoration and to see the effect of hot and dense conditions already at SIS energies by measuring particle spectra.

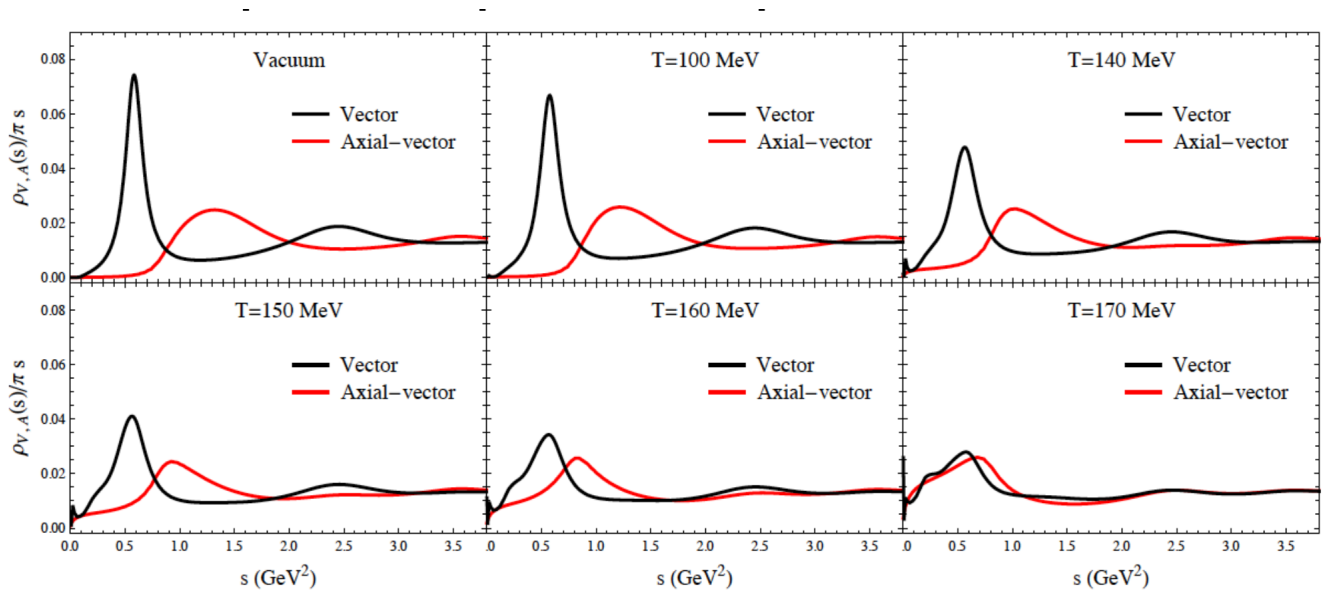

Figure 1.3: Evolution of chiral partners particle spectra with increasing temperature. Figure from [19].

1.2 Collisions of heavy ions at relativistic energies

In order to gain information about the QCD phase diagram and create hot and dense conditions, nuclei are collided in particle accelerators. In case of the HADES detector this is done with a fixed target. Measurements of particles coming from the collision give information about how the particles were created and in term what conditions were reached during the collision. The dominant interactions between the particles in a collision are, as desired, via the strong force.

1.2.1 Collisions - Centrality

One collision of two nuclei is called an event. As one can see in figure 1.4 events can differ depending on their impact parameter b. Small impact parameters correspond to a central collision while b closer to the maximum of $b_{max} = 2r_n$, r_n being the radius of the nucleus, are called peripheral collisions. In central collisions the participating zone, also called fireball, is larger and involves more particles which is why events for the analysis have to be distinguished depending on the centrality.

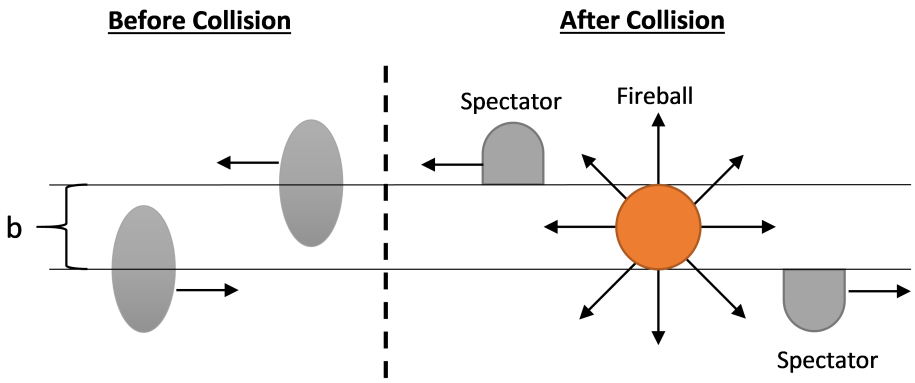

Figure 1.4: Impact parameter b illustration. One can see two relativistic nuclei colliding. After the collision spectators remain.

A detailed description on how an events centrality is determined as well as how centrality classes are defined for this work is in section 3.2.

1.2.2 Dileptons as collision probes

Direct measurement of the the fireball properties (i.e. T and ρ) is difficult for two reason. For one, the lifespan of the fireball and of rare particles created in the fireball is very short ($\sim 10^{-24}s$) which is why such particles cannot reach the detector before decaying. In addition, the mean free paths of strongly interacting particles, are too short to reach the detector unhindered. Instead they scatter and react with other strongly interacting particles such that hadrons finally reaching the detector have lost most of the information about the early stages of the fireball.

It is for this reason that lepton pairs, or dileptons, are often times better suitable candidates to reconstruct events in the fireball. The most dominant interaction for leptons is the electromagnetic force. Since the electromagnetic force is weaker relative to the strong force, the mean free path is large enough that leptons can reach the detector mostly undisturbed.

Electrons and their antiparticle positrons have the smallest mass of all charged particles measured in the experiment. They also have a number of different sources, namely via the decay of

virtual photons into a e^+e^- pair. Such pairs are called dileptons and are the collision products investigated in this work. In general a dilepton could name any kind of lepton paired with its antiparticle, but in this work it will be used as a synonym for e^+e^- pairs. This makes sense considering that these pairs are the most common lepton pairs at the investigated energies and other kind of lepton pairs are not taken into account for this analysis.

1.2.3 Dilepton sources

Depending on the beam energy as well the stage of a collision, there are different sources for dileptons. For energies investigated in this work this mainly includes Dalitz decays of pseudoscalar mesons or direct decays of vector mesons. The following table gives a brief overview of which dilepton sources are to be expected in the given energy regime:

Table 1.1: Dilepton sources for SIS energies - BR: Branching Ratio, J:Spin, P:Parity, I:Isospin. Table taken from [2].

Source	J^P	I	Mass [MeV/c^2]	Decay width [MeV/c^2]	[fm/c]	Product	[%]	e^+e^-	e^+e^- BR
Dalitz-Decays of the pseudoscalar mesons									
π^0	0^-	1	135	0.78	251	$\gamma\gamma$	98.8	γe^+e^-	1.2%
η	0^-	0	547	0.001	$\gg 30$	$\gamma\gamma$	39.4	γe^+e^-	0.5%
Direct decays of the vector mesons									
ρ	1^-	1	771	149	1.3	$\pi^+\pi^-$	100	e^+e^-	$4.6{\cdot}10^{-5}$
ω	1^-	0	782	8.44	23.4	$\pi^+\pi^-\pi^0$	89	e^+e^-	$7{\cdot}10^{-5}$
ϕ	1^-	0	1019	4.26	44.4	K^+K^-:	49	e^+e^-	10^{-5}-10^{-4}
Δ-Dalitz-Decay									
Δ	$(3/2)^+$	3/2	1232	115	1.7	Nπ	>99	N e^+e^-	$4{\cdot}10^{-3}$
Proton-Neutron-Bremsstrahlung: pn $\rightarrow$ pn e^+e^-									

Through these decays dileptons are created in all stages of the collision. Hence, the final signals measured in the experiment serve as an integral over the whole evolution of the colliding system. In this work, however, the interest lies in the hottest and densest phase, usually called the fireball. For this reason it should be mentioned which dilepton sources are most dominant throughout the different stages. In general three collision stages can be identified:

- **First-chance NN collisions:** Before all participating nucleons are involved it already comes to first chance nucleon-nucleon collision as the colliding ions start to overlap. In this stage dileptons are created via Bremsstrahlung and Δ Dalitz-decays.
- **Hot and dense fireball:** When temperatures and density reach their maximum, it is called the hot and dense fireball. In this stage, vector mesons ρ,ω and ϕ are created and eventually decay into dilepton pairs.
- **Freeze Out:** In time the system expands and cools down. The chemical freeze out names the point in which inelastic scattering stops. After some additional time the kinetic freeze out is reached in which elastic scatting also comes to an end. In this stage Dalitz decays of π^0 and η are responsible for dilepton production. In addition, vector mesons from the

fireball can decay in this stage because their lifetime can be longer than the lifetime of the fireball.

The ρ-meson is of particular interest for the analysis due to its short lifetime. This way it is the most likely vector meson to decay within the fireball and presents the best probe to study the hottest and densest stage. Furthermore it is also the most frequently produced vector meson.

Looking at all decay channels it should be noted that the branching ratio for dilepton production is usually relatively small. Hence, a large number of events as well as high efficiency and acceptance is needed in order to gain enough statistics in the analysis.

Finally, the table already indicates one way that measurement of dileptons carries information about the collision. When counting the number of dilepton pairs and their mass in a collision, it is possible to make an estimate of the number of corresponding source particles. Such ideas shall be underlined, as even though leptons do not interact strongly, they carry information about strongly interacting particles.

1.3 Former analysis and motivation

Reconstruction of virtual photons as a tool to study heavy ion collision has been used worldwide and is one of the main research topics at the HADES detector. Since dileptons are produced at basically all beam energies and for any number of participating nucleons, there are many aspects that can be investigated using dileptons. At HADES different collision systems at the low energy range ($\approx 1 GeV/u$) have been and are continuously studied. In particular, in [1] and [3] virtual photons for Au+Au collisions at $1.23 GeV/u$ have been reconstructed.

In most cases however, only central events (usually from 0-40% centrality) are investigated. This is mainly because the number of particles declines with decreasing centrality which means worse statistics. This work aims to build on these works and include more peripheral events in the analysis. It is to be inspected whether statistics are good enough to pursue peripheral events analysis in the future. This is important as such events are needed for a more complete picture of the fireball and they could even give insight on phenomena which so far remained hidden or unexplained. Furthermore, peripheral events could serve as a verification for existing models and theories.

To be more precise, the goal of this work is to produce invariant mass spectra of e^+e^-pairs for peripheral events and if possible start to extract physical properties about the fireball from the results.

2 HADES

Before the actual analysis can be made, is is important to discuss the experimental setup used to gain the experimental data. The data for this work stems from the High Acceptance Di-Electron Spectrometer (HADES) at GSI, Darmstadt. In the following sections the most key detector elements shall be described briefly.

2.1 Target and start detector

The first element is a fixed Au target on which the accelerated Au ions are fired. It is made up out of 15 thin metal foils which are positioned one after another [6].

Directly in front of the target, within the beam line, is the start detector which creates a signal for every beam particle flying through the target. These signals act as start time of an event and can later be used to calculate time of flight and velocity of a given particle. Furthermore, the spacial resolution of the detector is used to focus the particle beam. Since many particles reach the detector in short succession, high temporal resolution is required and was about 54ps [15] for this experiment.

2.2 Particle Tracking system

The main tools for track reconstruction in HADES is the Multiwire Drift Chamber (MDC). The MDC consists of several gas filled cells in which a multitude of parallel wires are set up. Every wire serves as an anode and creates an electric field. Charged particles flying through the cell leave a trail of ionized gas atoms and free electrons that are accelerated towards the anode. The electrons gain kinetic energy and via scattering processes create secondary electrons. It comes to an avalanche effect and the electrons reaching the wire can be measured as an electric signal. A single chamber has 6 overlaying cells, each at an angle to each other, such that several anodes register a signal and it is possible to locate the place of origin from the intersection. This way the MDCs have spatial resolution. In addition, the energy loss of a passing particle can be calculated using the signal width. This information proves useful later when trying to distinguish particle types.

At HADES there are 4 MDCs in total, two being before a superconductive magnet and two being behind it. This way it is possible to calculate a particles trajectory before and after passing through the magnetic field. Comparing the two trajectories gives information on how far the particle was bent in the magnetic field. Since the Lorentz force that acts on the particle within the magnetic field is dependent on the particles momentum, this setup can be used to determine momenta and consequently a particles mass.

2.3 Multiplicity Electron Trigger Array

Behind the secondary pair of MDCs is a final set of detectors that are commonly referred to as META (Multiplicity Electron Trigger Array) detectors. For polar angles of roughly $\phi \geq 45°$ the Time of Flight (TOF) detector is placed while for smaller polar angles the Resistive Plate Chambers (RPC) as well as the Pre-Shower Detector are located. In order to distinguish between those systems, the former detector will be referred to as **system 1** and the latter as **system 0**. This separation is important as information about a particle is different depending on what system was hit.

2.3.1 Time of flight detector and resistive plate chambers

The time of flight detector (TOF) as well as the resitive plate chambers (RPC) are used for time of flight measurements by comparing the time of a registered signal with the start times given by the START detector. Since the distance covered by the particle during the time of flight is known, this allows to calculate a particles velocity. The main difference between the detectors are the processes which they use for measurements. While the RPC, as the name suggests, uses resistive plate chambers the TOF detector is based on scintillator technology. The RPC, on the one hand, is able to handle higher multiplicities while at the same time providing a high time resolution. The TOF detector, on the other hand, is not meant for high particles multiplicities since it is located at larger polar angles. However, using the TOF signal amplitude it is possible to make an estimate of the energy loss, something not possible at the RPC.

2.3.2 Pre Shower Detector

The Pre-Shower detecor is located behind the RPC and is an important tool for lepton identification. As depicted in figure 2.1 it consists of three gas filled chambers and two Pb partition walls. When a particle flies through the lead, it slows down and the deacceleration causes emission of Bremsstrahlung. The created photons have high enough energies to react with the Pb via pair production. Therefore, even more electrons and positrons are created and a showering effect can occur. It can be measured by comparing the amount of ionizing particles between each of the chambers.

However, the acceleration, and in term the amount of Bremsstrahlung emitted, is proportional to the inverse mass squared ($\propto Z^2 \cdot E/m^2$ [7]). Doing the calculations, it turns out that the energy loss for protons and heavier particles is negligible which is why for such particles no showering effect can be measured. Only the lightest particles, namely electrons and positrons, produce enough Bremsstrahlung, for a showering effect to occur. Hence, the Pre-Shower detector serves as another tool to identify such particles.

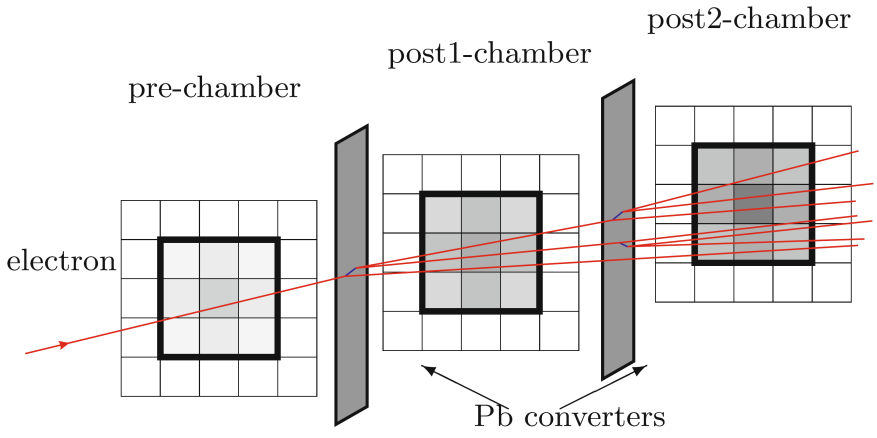

Figure 2.1: Pre-Shower Detector illustration. Figure taken from [17].

2.4 Ring Imaging Cherenkov Detector

The RICH detector is a key component of HADES for e^+/e^- identification. It is based on the Cherenkov radiation which is emitted by charged particles when travelling through a dielectric medium faster than light. This condition can be formulated as in Eq. 2.1 [7]:

$$c = \frac{c_0}{n} \leq \beta c_0 \implies E_{th} = \frac{mc^2}{\sqrt{1-\frac{1}{n^2}}} \tag{2.1}$$

with c: phase velocity of light in medium; c_0: speed of light in vacuum; n: refractive index of the medium; m: particle mass; E_{th}: threshold energy for Cherenkov radiation

From Eq. 2.1 one can see that the threshold energy grows with larger masses. Hence, the lightest, charged particles in the detector, which are electrons and positrons, fulfill condition Eq. 2.1 at smaller energies than heavier particles. With the knowledge of average and maximum energies at HADES, one can choose n in such a way that only electrons and positrons emit Cherenkov radiation.

This effect is used in the RICH detector. Is is made up of a gas chamber containing C_4F_{10} with a suitable refractive index of $n = 1,00151$ [2]. As depicted in figure 2.2 it covers a wide polar angle, so all particles reaching the HADES detector are registered. At its edge, a spherical mirror is located. While the collision particles can penetrate this mirror, it is highly reflective for the Cherenkov radiation photons. The reflected photons are finally measured at the photon detector. Simple geometry allows to reconstruct what way the photons came from.

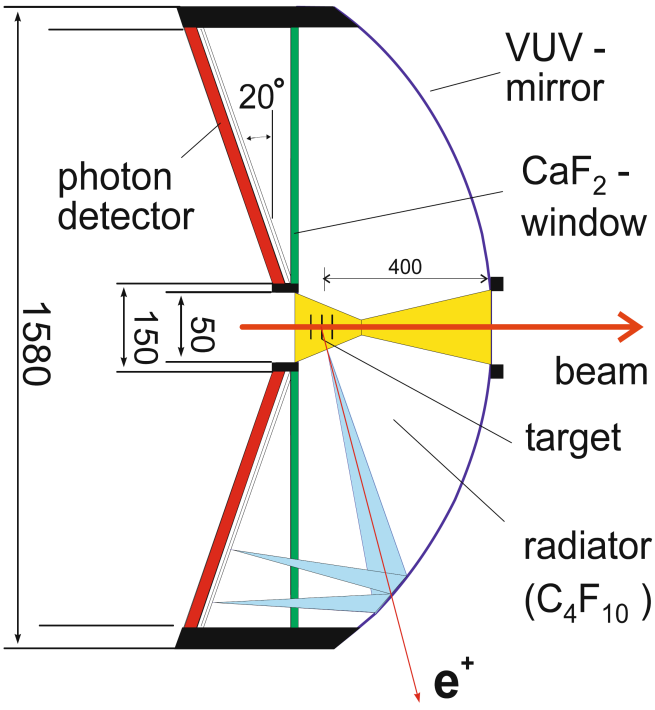

Figure 2.2: RICH Detector illustration. Figure taken from [17].

3 Event selection

The experimental data used in this work is based on measurements made by HADES in April 2012 colliding Au+Au at center of mass energy of 2.42 GeV. First, the raw data gathered has to undergo a procedure of being translated into physical properties, e.g. charge, momentum, velocity, and particles and their trajectories have to be reconstructed. The results are saved in Data Summary tape (DST) files. The DST can then be used individually for whatever analysis is of interest.

The DST is structured in a tree with a list of classes that might be interesting for an analysis. This work for one uses a class that includes all the events and their classifications measured during the beam time. Another important class lists all particles reconstructed for a given event. Every particle is also assigned a list of properties. It should be noted that the tracks reconstructed for the DST serve as best guesses and are not flawless. This is why selection criteria have to applied such that the remaining particles can be assumed to be genuine.

3.1 Event Selection Conditions

With the DST one can loop over all events and perform the desired analysis. However, not all events are equally suitable for dilepton analysis. For one, two events could have been in such short succession that they are counted as one event. This phenomena is named pile up event and could potentially distort the results of the analysis. Furthermore, some events could have high background noise or incorrect time measurements. The latter would lead to wrong time of flight estimations which would in term alternate all kinds of calculated observables while the former are unsuitable for precise analysis.

Therefore, one needs to filter for high quality events in order to gain reliable results. The conditions used for this work are listed in the following [1][3]:

- **goodStart:** Removes events that do not have a well defined start time.
- **noPileUpStart:** Removes events if a second cluster has been detected by START, in order to prevent pile up events.
- **NoVeto:** Removes nuclei that signaled in START detector but did not collide with target.
- **goodSTARTVETO:** Removes events in which an additional START hit occurred within 15-350 ns for which there is no correlated VETO hit in the windows $+-2ns$
- **goodSTARTMETA:** Removes events in which an additional START hit occurred after 80 - 350 ns which is also correlated to META hits.
- **goodVertex:** Removes collision events that are not Au+Au, e.g. collisions of beam nuclei with surrounding material, by reconstruction of reaction vertices.

These conditions shall be summarized as "**isGoodEvent**" for future reference.

A last condition is not directly event related but instead stems from experimental experience. The HADES detector consists of 6 equal sectors. However, it is not uncommon for one or more sectors to fail occasionally and provide no or faulty data. If this is the case, the affected sector has to be removed from the data sample. This however, changes the acceptance of the detector and has to be taken into account when comparing the experimental data with theoretical predictions.

It is also easy to realize that the analysis becomes less precise the more sectors are missing. For this reason a function is implemented which takes into account necessary sector corrections. In particular it removes events in which less than four active sectors:

- **chooseSectorCorr:** Removes events with less than four active detector sectors.

3.2 Centrality Selection

After filtering the events for high enough quality, another distinction can be made between them. As mentioned in section 1.2.1, events can be separated into different centrality classes depending on their impact parameter b. Since this work focuses on peripheral events and the size of the participating zone is centrality dependant, it makes sense to sort events into different categories depending on their centrality. However, b is not an observable that can be measured directly during the experiment. For the definition of centrality classes one instead looks at the number of Meta-hits N_{Meta}. It is believed that the number of charged particles N_{ch} created in an event is proportional to the number of participants A_{part} involved in the collision [1]:

$$A \propto N_{ch} \tag{3.1}$$

Furthermore, the number of charged particles N_{ch} is correlated to the number of Meta hits N_{Meta}. Since A_{part} is dependent on the impact parameter b, measurement of N_{Meta} provides a way of differentiating between centrality classes. The definitions of centrality classes, using the number of meta hits N_{Meta}, for this work are summarized in table 3.1 and are based on Glauber Monte Carlo simulations [12]:

Table 3.1: Centrality classes definitions from HADES for Au+Au at $\sqrt{s_{NN}} = 2.42\ GeV$.

Centrality[%]	$\langle b \rangle$	$\langle A_{part} \rangle$	$\Delta\langle A_{part} \rangle$	N_{Meta}
0-10	3.14	303.0	22.35	161.00 - 275.00
10-20	5.7	213.1	19.7	123.00 - 161.00
20-30	7.38	149.8	17.15	91.00 - 123.00
30-40	8.71	103.1	13.03	64.00 - 91.00
40-50	9.86	68.4	12.27	43.00 - 64.00
50-60	10.91	42.3	5.62	27.00 - 43.00
60-70	0.00	27.00		0.0 - 27.00

3.3 Physics triggers

At HADES a dedicated trigger system is used to determine whether a measured signal is to be stored. The most important ones to understand this work are the so called physics triggers (PT) 2 and 3. They are requirements on the minimal hit multiplicity measured at TOF for a given event. More precisely, a PT2 event has at least 6 and a PT3 event at least 20 hits registered at the TOF detector. This distinction is made because while every PT3 event is stored, only every eight PT2 event is stored; a process which is called down scaling.

As this work includes peripheral events however, one has to include PT2 events in the analysis. In theory scaling the PT2 events with a factor of 8 should lead to an equal distribution of events between each centrality class. Yet it turns out, that this is not the case and a scaling factor of

eight leads to a larger number of peripheral than central events. It was discovered that the main reason for this is because the factor of how many PT2 events are stored during the experiment was changed from 4 to 8 at the end of day 105 of year 2012 in midst of the experiment.

Therefore, in this work PT2 and PT3 events have firstly been counted in two separate histograms, as shown in figure 3.1:

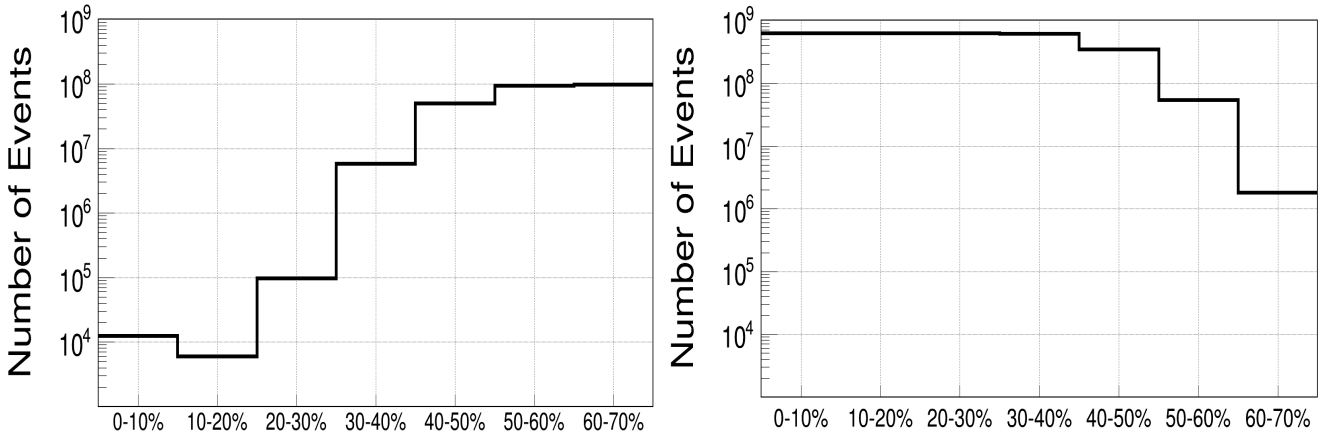

(a) PT2-Event Counter **(b)** PT3-Event Counter

Figure 3.1: Event Counter for different centrality classes and the two physics triggers. Data from HADES for Au+Au at $\sqrt{s_{NN}} = 2.42\ GeV$.

One can see how the number of PT2 events get larger with increasing centrality while it is the other way round for PT3 events. In order to gain a scaling factor the PT2 events counter histogram has been added to the PT3 events counter histogram with different weighting. Through trial and error a **scaling factor of 6** has been concluded to show satisfactory equal distribution between all centrality classes. The results are shown in the following:

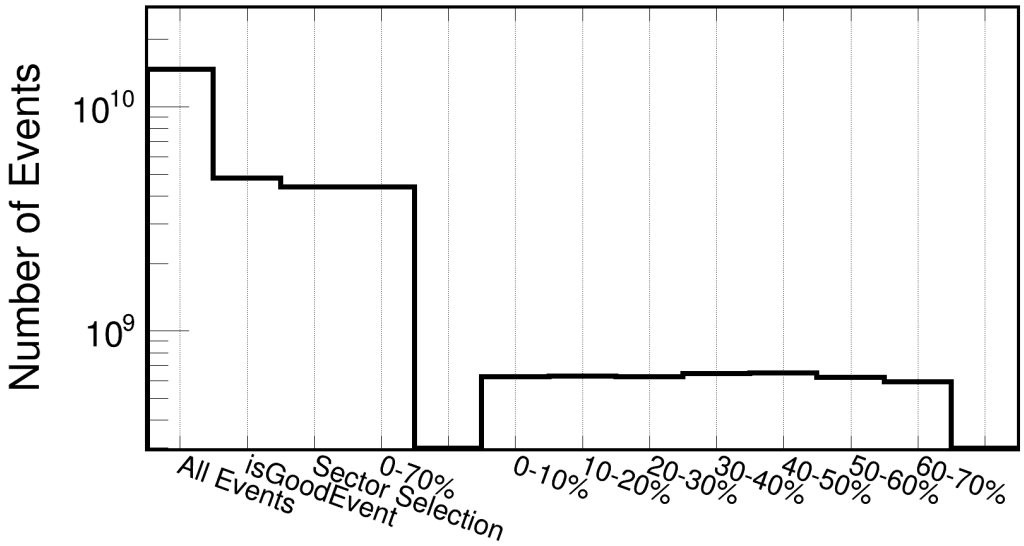

Figure 3.2: Event Counter from HADES for Au+Au at $\sqrt{s_{NN}} = 2.42\ GeV$. It can be seen how the number of events are filtered by the event selection. The points to the right show a roughly equal distribution of events over the different centrality classes.

4 Lepton identification

In the next step of the analysis the leptons which are to be investigated, have to be separated from other particles. This is a balancing act since on the one hand, one wants as many leptons as possible, in order to have better statistics for the analysis, but on the other hand, one has to make strict cuts to make sure as many hadrons as possible are removed from the sample.

In a simple manner, using the fact that electrons/positrons are the lightest charged particles in the experiment, one can immediately setup some conditions which leptons would need to fulfil. In the analysis they are summarised in the function "**selectLeptonsBeta**" which includes the following requirements [3]:

- The upper limit for the velocity is $\beta = 1.1$ and the lower limit is $\beta = 0.95$ and $\beta = 0.92$ for system 0 (RPC+Pre-Shower) and for system 1 (TOF) respectively.
- The reconstructed track aligns with a corresponding hit in a time of flight detector.
- The energy loss must not be higher than a given threshold.
- The Runge-Kutta fit for the track reconstruction gives a $\chi^2_{RK} < 100$.
- The particles momentum p is between 100 - 1000 MeV/c.
- The particles track is not marked as fake in the track reconstruction procedure.
- Particle track has a corresponding signal at the RICH detector.

One can notice that these conditions not only serve as lepton selection tools, but also include requirements for the general track quality of a candidate such that fake hits are prevented.

All in all, this already removes many unwanted particle candidates. It should be underlined that the RICH detector is of central importance for the lepton identification. To gain a better efficiency, particle candidates are preselected and must go through the other listed conditions first. Then the track of a given particle candidate is used to calculate a region of interest within the RICH detector where a corresponding signal could be. Only then information from RICH measurements are taken into account to determine whether a signal within the region fits with the candidates track. This procedure is called backtracking, as it takes additional tracking information, and is explained in more detail in [16].

Unfortunately hadrons may coincide with a nearby lepton which leads to the RICH detector being not perfectly hadron blind and the resulting pool of particles is still impure, meaning a not negligible number of hadrons fulfil the listed conditions too. For a better result, a more sophisticated tool must be implemented.

4.1 Multilayer Perceptron

One of the problems of precisely defined cuts, e.g. as in section 4, is the fact that they are taken one after another and correlations between them are ignored. This may be problematic, as for example it may be possible that an electron fulfills every condition except one where it lays just beyond a given threshold. Since the thresholds are fixed, this electron would then be

removed and one would miss out on better statistics. Lowering this threshold however, so that this electron would be recognized as such, could lead to more hadrons which are falsely counted as an electron.

Hence, a multilayer perceptron (MLP) is implemented. It acts as a neural network that takes into account a whole set of physical quantities simultaneously in order to come to the single conclusion whether a given particle is a lepton or not. Such a procedure of using a set of variables to gain one output is called a mutlivariate analysis (MVA). The most definite advantage of this method is the possibility to pay attention to correlations between the observables.

The input variables are listed in the following [3]:

- Velocity β
- Energy loss dE/dx
- Momentum p
- Polar angle of emission θ
- META matching quality, more precisely how well the track and corresponding META hit align.
- Information from RICH detector.

Depending on what system of the META detector is hit by the particle, additional information can be included. An example for this is the information from the Pre-Shower detector when the particle hit system 0. A more detailed description about the working of the MLP can be found in [3]. The key point for this work is that this procedure provides an adequate balance in getting a large but pure pool of dileptons and is consequently used for this analysis.

4.2 Close pair rejection

Not all leptons identified are of interest in the analysis. Many leptons are created when photons from the collision interact surrounding detector material via pair production. Such leptons carry no information about the decays of collision particles and as such, act as irrelevant background which has to be removed. The easiest way to reduce this effect is to implement a close pair rejection cut which is based on the following estimation [5]:

$$\theta_{oangle} \approx \frac{0.8}{E_\gamma} \tag{4.1}$$

whereas E_γ is the photon energy and θ_{oangle} is the opening angle between the created positron and electron.

Large Energies E_γ lead to small opening angles which is why it is checked whether there is a conversion partner near an identified electron (analogously for identified positron). In such a case the lepton will be removed form further analysis as it is most likely uninteresting background. Since θ_{oangle} is small, possible conversion partners often share a RICH detector signal with the electron. Therefore, tracks, reconstructed with MDC and META, are taken into account to search for such phenomena. A more detailed explanation as well as a list of observables used for this procedure can be found in [3].

4.3 Resulting Sample

Applying the lepton identification as described above creates a sufficiently pure sample of leptons. The effect can be seen quite nicely when looking at the a plot of the velocity β versus charge times momentum, as seen in figure 4.1 in the example of system 0.

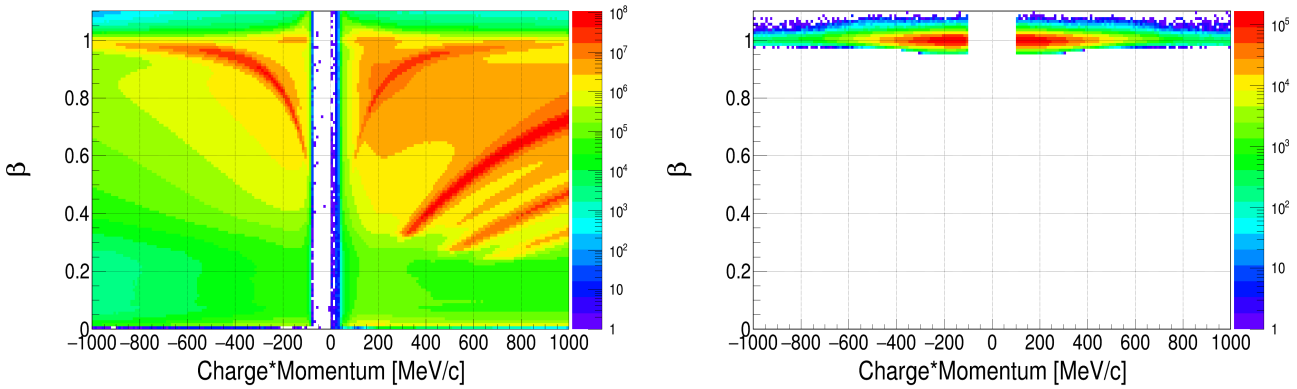

(a) Before Lepton Identification **(b)** After Lepton Identification

Figure 4.1: Number of particles over charge momentum and velocity before and after lepton identification and selection. The data shown is using particles that hit system 0 (RPC+Pre-Shower) and is from Au+Au collisions, 0-70% centrality at $\sqrt{s_{NN}} = 2.42\ GeV$, HADES.

Furthermore one can study the number of events over the number of e^+ and e^-, as it is done in figure 4.2 for the most central and most peripheral centrality class investigated in this work. For better visibility the bins (0:0),(0:1) and (1:0) are suppressed because such events do not contribute to pair analysis. Since the total number of events is roughly equal throughout all centralities (see section 3.3), it can be seen that the number of leptons decreases with increasing centrality. In addition, it can be noted that there are always more electrons than positrons measured in the experiment. This indicates a charge asymmetry in the detector which should be taken into account in the rest of the analysis.

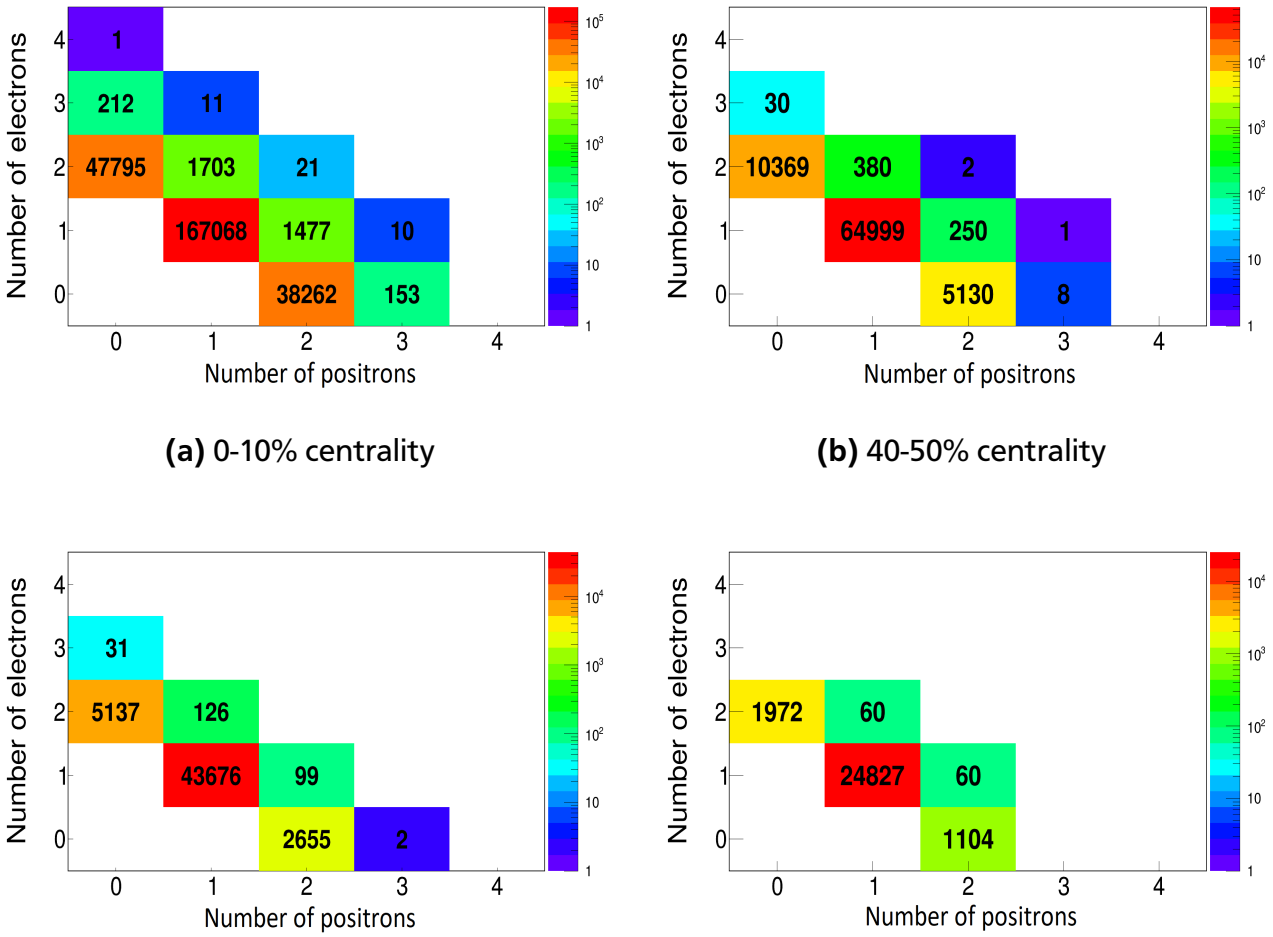

(a) 0-10% centrality

(b) 40-50% centrality

(c) 50-60% centrality

(d) 60-70% centrality

Figure 4.2: Number of events over e^+/e^- multiplicity. (Au+Au at $\sqrt{s_{NN}} = 2.42\ GeV$, HADES)

5 Combinatorial background

After the event and lepton selection, the actual analysis and filling of invariant mass spectra can begin. After two leptons have been identified as a pair, their invariant mass $M_{e^+e^-}$ is given by the sum of their 4-momentum vectors [3]:

$$M^2_{e^+e^-} = (E_{e^+} + E_{e^+})^2 - (\vec{p_{e^+}} + \vec{p_{e^-}})^2 \tag{5.1}$$

with the momentum vector $\vec{p}$ and the energy E of each the electron and positron. The invariant mass of two same-sign lepton pairs is calculated analogously.

Now the main difficulty lies in deciding which electrons and positrons actually belonged together and formed a pair. Since there is no way of confidently deciding this, another more indirect route is taken.

Allowing multiple combinations for one lepton, one first makes a invariant mass spectra of all possible electron-positron pairs $\frac{dN_{+-}}{dM}$ in a given event. The actual signal $\frac{dN_{Signal}}{dM}$ can then be calculated by subtracting the combinatorial background (CB) $\frac{dN_{CB}}{dM}$ [9]:

$$\frac{dN_{Signal}}{dM} = \frac{dN_{+-}}{dM} - \frac{dN_{CB}}{dM} \tag{5.2}$$

Now the difficulty of deciding which pairs belong together is encoded in the CB. Hence, the following section shall discuss how this is calculated.

5.1 Estimation of combinatorial background

The most common way of calculating the combinatorial background in dilepton analysis is the so called Same Event like-sign method.

In addition to the unlike-sign pairs $\frac{dN_{+-}}{dM}$ one also fills spectra with like-sign pairs of electron-electron $\frac{dN_{--}}{dM}$ and positron-positron $\frac{dN_{++}}{dM}$. It can be shown that the Same Event background $\frac{dN_{CB_{SE}}}{dM}$ can than be calculated using the geometric mean [10]:

$$\frac{dN_{CB_{SE}}}{dM} = 2\sqrt{\frac{dN_{++}}{dM} \cdot \frac{dN_{--}}{dM}} \tag{5.3}$$

The biggest advantage of this method is the fact that it includes correlated, as well as uncorrelated background. However, using only Eq. 5.3 for the calculation is not ideal.

Firstly, for Eq. 5.3 perfect charge symmetry in the detector is assumed. This means that electrons and positrons are either equally likely to be detected and reconstructed or acceptance and efficiency charge asymmetry coincidentally cancel each other out such that in total the detector appears to be charge symmetric. However, as seen in section 4.3, one can recognize a charge asymmetry from the detector and particle reconstruction.

Secondly, the Same Event method has very limited statistics as very few pairs are created in a single event. Especially for higher invariant masses this leads to relatively large statistical errors and possibly point-to-point fluctuations which is why the CB estimation becomes less precise.

For these reasons a second method, called the event-mixing method, is used additionaly in an attempt to eliminate these issues.

In the event-mixing method pairs of leptons, stemming from separate events, are created. This is illustrated in figure 5.1. For notation the spectra of unlike pairs for mixed event shall be noted as $\frac{dN_{+-}^{mix}}{dM}$, of e^+e^+ pairs as $\frac{dN_{++}^{mix}}{dM}$ and of e^-e^- pairs as $\frac{dN_{--}^{mix}}{dM}$.

The main advantage of such a procedure is the possibility of virtually unlimited statistics, as one can freely choose how many events are to be mixed. At the same time, however, it only allows for estimation of uncorrelated background.

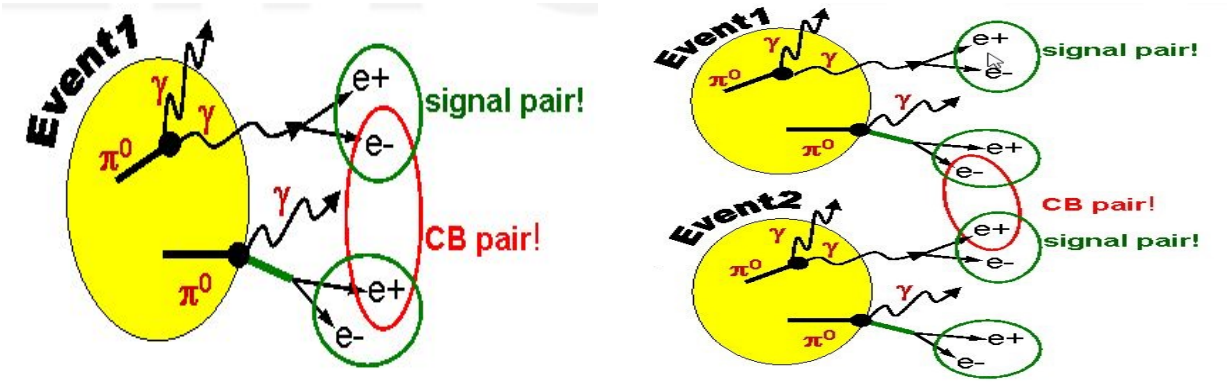

(a) Same Event method. **(b)** Mixed Event method.

Figure 5.1: Methods to calculate combinatorial background illustration. Figure from: `https://hades-wiki.gsi.de/foswiki/bin/view/Homepages/Dielectrons` (accessed 26.06.2018)

With these methods including their advantages and disadvantages in mind, one can combine both methods to gain the estimate of the CB. Firstly, the event-mixing method is used to calculate a k-factor which accounts for charge asymmetry:

$$k = \frac{\frac{dN_{+-}^{mix}}{dM}}{\sqrt{\frac{dN_{++}^{mix}}{dM} \cdot \frac{dN_{--}^{mix}}{dM}}} \tag{5.4}$$

Using this factor one can correct formula Eq. 5.3:

$$\frac{dN_{CB_{SE}}}{dM} = 2k\sqrt{\frac{dN_{++}}{dM} \cdot \frac{dN_{--}}{dM}} \tag{5.5}$$

This has proven to be a good estimate of the CB and with Eq. 5.2 it is possible to calculate the actual signal of dileptons measured in the experiment.

The amount of dileptons decreases for larger masses and the limited statistics become more problematic. Assuming that the CB is mostly uncorrelated for such mass regions, it would be better to use the event-mixing method to estimate the CB since that would allow for better statistics. In order to check this assumption, the ratio $\frac{dN_{CB_{SE}}}{dM} / \frac{dN_{+-}^{mix}}{dM}$ is calculated. As shown in figure 5.2 the ratio stays constant within errors for invariant masses of $M_{ee} > 0.4\ GeV/c^2$.

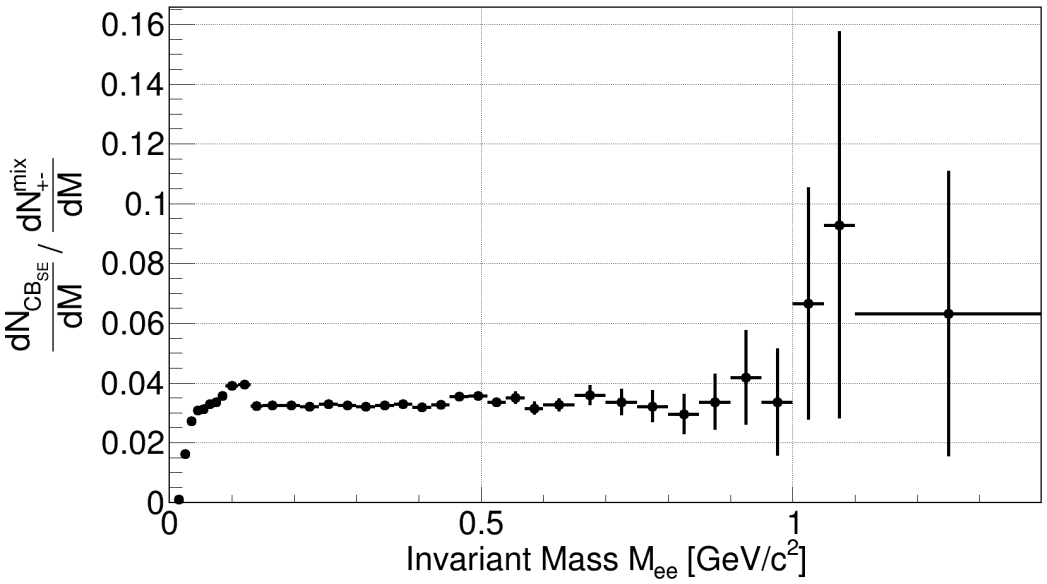

Figure 5.2: Same Event/Mixed Event combinatorial background ratio (Au+Au 0-70% centrality at $\sqrt{s_{NN}} = 2.42\ GeV$, HADES). It can already be seen that the statistical errors become larger with increasing mass due to the limited statistics for the Same Event background. In addition, one can note a local maximum at about $M_{ee} = 0.1\ GeV/c^2$.

This means that the shapes are the roughly the same and as logical conclusion that the CB is overwhelmingly uncorrelated for higher mass regions. This knowledge allows the usage of $\frac{dN^{mix}_{+-}}{dM}$ as an CB estimation such that statistical errors can be reduced. For normalization the Same Event calculations are used:

$$\frac{dN_{CB_{ME}}}{dM} = \frac{dN^{mix}_{+-}}{dM} \cdot \frac{\int_{0.3GeV/c^2}^{0.4GeV/c^2} \frac{dN_{CB_{SE}}}{dM} dM}{\int_{0.3GeV/c^2}^{0.4GeV/c^2} \frac{dN^{mix}_{+-}}{dM} dM} \tag{5.6}$$

Using Eq. 5.5 for $M_{ee} < 0.4\ GeV/c^2$, and Eq. 5.6 for the remaining mass spectrum, the CB for every centrality class has been calculated and the signals extracted.

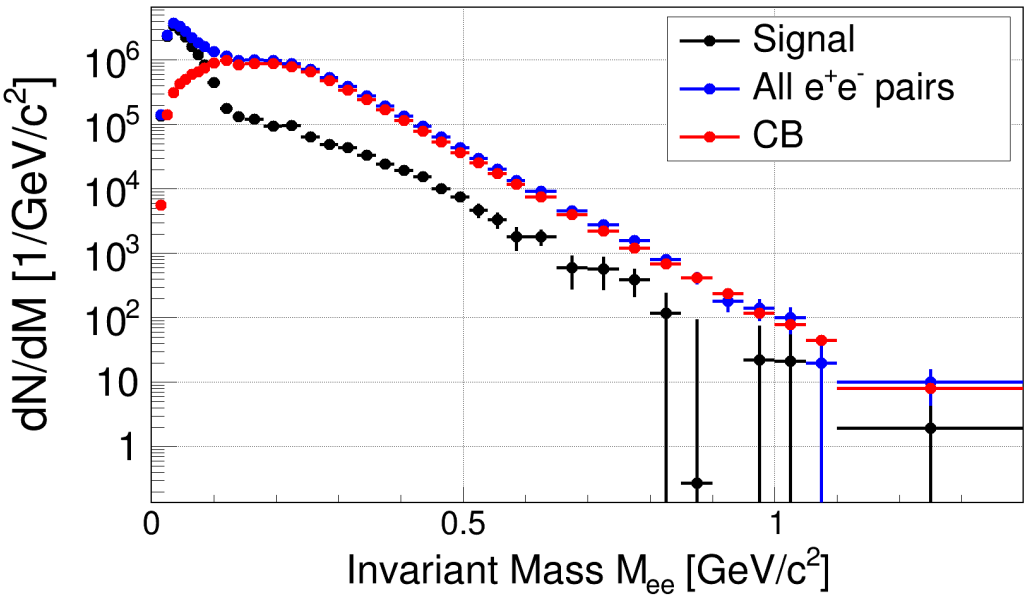

Figure 5.3: Example of combinatorial Background subtraction and the resulting signal. The errors bars represent the statistical errors. (Au+Au 0-70% centrality at $\sqrt{s_{NN}} = 2.42\ GeV$, HADES)

5.2 Estimation of possible physics trigger bias

As mentioned in section 3.3 PT2 events have to be weighted with the appropriate scaling factor when filling histograms. In case of the Same Event method this is trivial, either an event had a PT3 and no additional scaling has to be done, or an event had an PT2 and the histogram can simply be filled with a weight of 6. In contrast PT scaling for mixed events proves to be more complex, because the paired leptons may come from events which have different physics triggers assigned to them. In fact there a three possibilities:

1. Both leptons come from a PT3 event. (Notation: PT33)
2. Both leptons come from a PT2 event. (Notation: PT22)
3. One lepton comes from a PT2 and the other one from a PT3 event. (Notation: PT23)

In a first step several histograms were created, one for each case separately. This way one can add the histograms later with whatever scaling one wants to assign to each case.

Furthermore, since the event mixing has to be normalized anyway, see Eq. 5.6, weighting is only important if the histograms for the different PT events have different shapes. This can be checked by calculating the ratios between the different histograms. As an example the results for 40-50% centrality are shown because in this centrality class this is the region where PT3 as well as PT2 events are common.

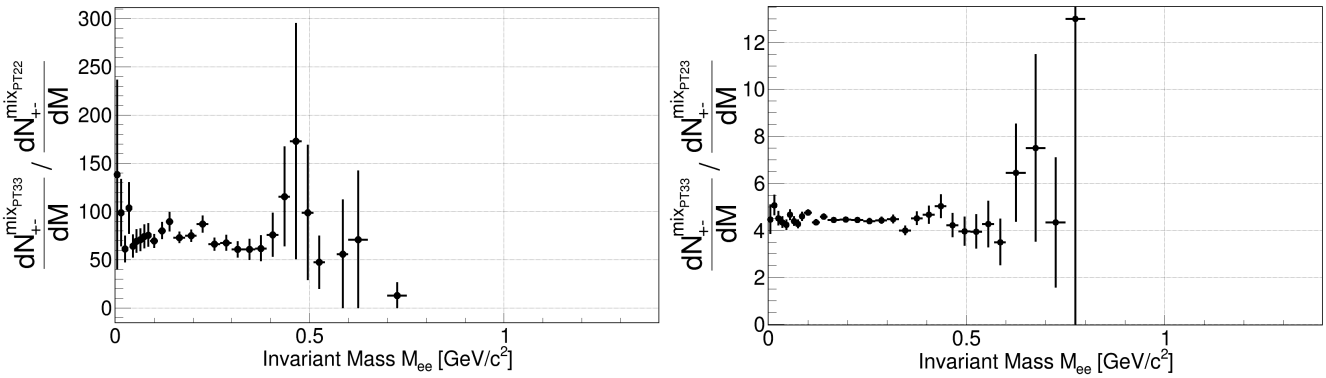

(a) PT33/PT22 **(b)** PT33/PT23

Figure 5.4: PT-Ratios for mixed events (Au+Au 40-50% centrality at $\sqrt{s_{NN}} = 2.42\ GeV$, HADES).

It can be seen that the ratios are constant as an adequate approximation.

This is less true when looking at figure 5.4a as one can recognize a deviation from a constant ratio. However, one should also note that the relative portion of PT22 events is mostly under 2%. This is why these deviations shall be ignored and for the purposes of this analysis it is assumed that the shapes are independent of the physics trigger assigned to an event. Hence, no further PT scaling has been done for the event mixing.

6 Efficiency and Acceptance Corrections

With the methods described in section 5 invariant mass spectra for different centrality classes are created. But, these do not account for detector and track reconstruction efficiency. In order to make statements about the actual properties of the fireball and to be able to compare results with other theories or experiments, the spectra have to be corrected first.
In general two types of corrections are differentiated:

Acceptance corrections come from the fact that the detectors cover a limited solid angle Ω and many, e.g. structural, parts of the detector are not capable of particle registration. For this reason, some leptons are missing in the measured data. If one wants to know how many leptons were actually created one has to correct for acceptance. Let N_{Acc} be the number of leptons reaching an active detector and N_{Total} be all leptons stemming from the collision, then the acceptance ϵ_{Acc} can be calculated by [3]:

$$\epsilon_{Acc} = \frac{N_{Acc}}{N_{Total}} \tag{6.1}$$

In addition there are efficiency corrections. Even when leptons fly through active detector parts, there is no guarantee that they will be reconstructed properly or that they will be identified as leptons. Hence, efficiency corrections have to be made to account for loses in track reconstruction as well as lepton identification. The latter is needed because the lepton identification is not flawless and some leptons will be falsely removed from the sample. Let N_{reco} be the number of leptons reconstructed and identified then the efficiency ϵ_{Eff} can be calculated by [3]:

$$\epsilon_{Eff} = \frac{N_{reco}}{N_{Acc}} \tag{6.2}$$

Even though in the reconstruction of virtual photons only lepton pairs are investigated, single lepton efficiencies have to be calculated first.

Based on the experimental data alone it is impossible to correct the signals, since N_{Total} as well as N_{Acc} are unknown and have to be estimated. One way of doing this is to simulate a large number of leptons with random values for momentum p as well as azimuth Θ and polar angles Φ. These leptons are then embedded into UrQMD which simulates an event including all manners of particle interactions. In case of efficiency calculations the results undergo the same track reconstruction and lepton identification as the original experimental data. Due to the leptons being simulated, their total number is known and efficiency as well as acceptance can be calculated according to Eq. 6.1 and Eq. 6.2. In this way one can create acceptance and efficiency matrices as a function of (p, Θ, Φ).

In a second step dilepton pairs are simulated to fill an invariant mass spectrum. For the acceptance corrections this invariant mass spectrum is simulated for the whole solid angle of 4π and shall be noted as $\frac{dN^{4\pi}}{dM}$. Then these simulated leptons are corrected with the known acceptance matrises and with the corrected leptons a new invariant mass spectrum $\frac{dN^{acc}}{dM}$ is filled. Like in Eq. 6.1 the acceptance correction is then given by the ratio of $\frac{dN^{acc}}{dM} / \frac{dN^{4\pi}}{dM}$. The results are plotted in the following figure:

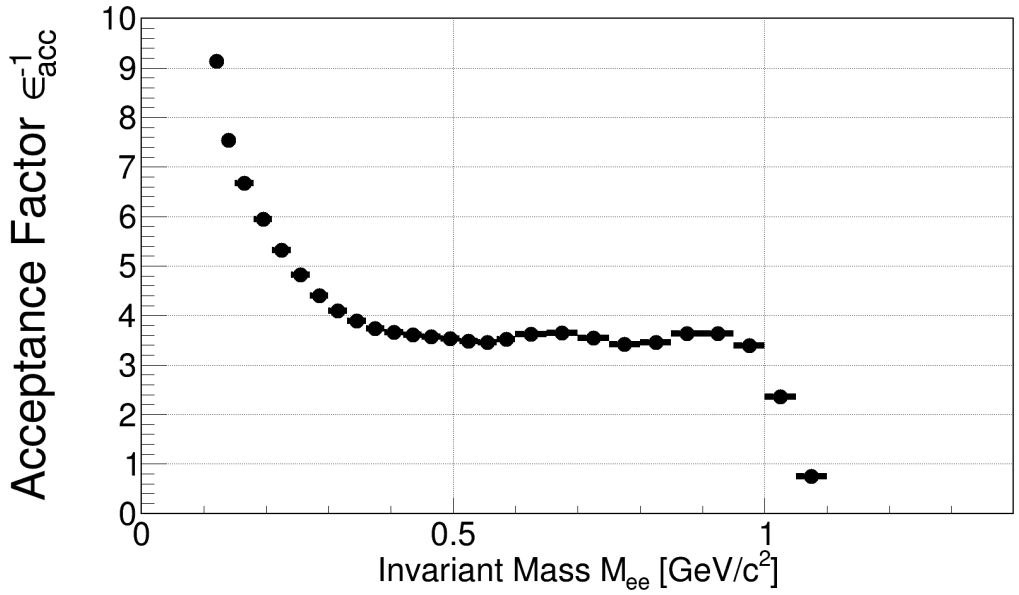

Figure 6.1: HADES Acceptance Corrections for Au+Au at $\sqrt{s_{NN}} = 2.42\ GeV$.

Similarly the efficiency can be calculated taking the leptons from $\frac{dN^{acc}}{dM}$ and correcting these with the efficiency matrices. The corrected leptons are then used to fill another invariant mass spectrum $\frac{dN^{reco}}{dM}$ and the efficiency is calculated like in Eq. 6.2 by taking the ratio $\frac{dN^{reco}}{dM}/\frac{dN^{acc}}{dM}$.

6.1 Centrality dependence

The acceptance is purely based on the detector setup and as such only has to be calculate once. The limited efficiency on the other hand is among other things caused by the difficulty of reconstructing tracks. This issue is more dominant for events with high multiplicities that is why the efficiency is ultimately centrality dependent. For centrality classes between 0-40% this is taken into account by simply calculating the efficiency for every class separately. The result is shown in figure 6.2 where the inverse of ϵ_{Eff} is taken to get an efficiency factor ϵ_{Eff}^{-1}:

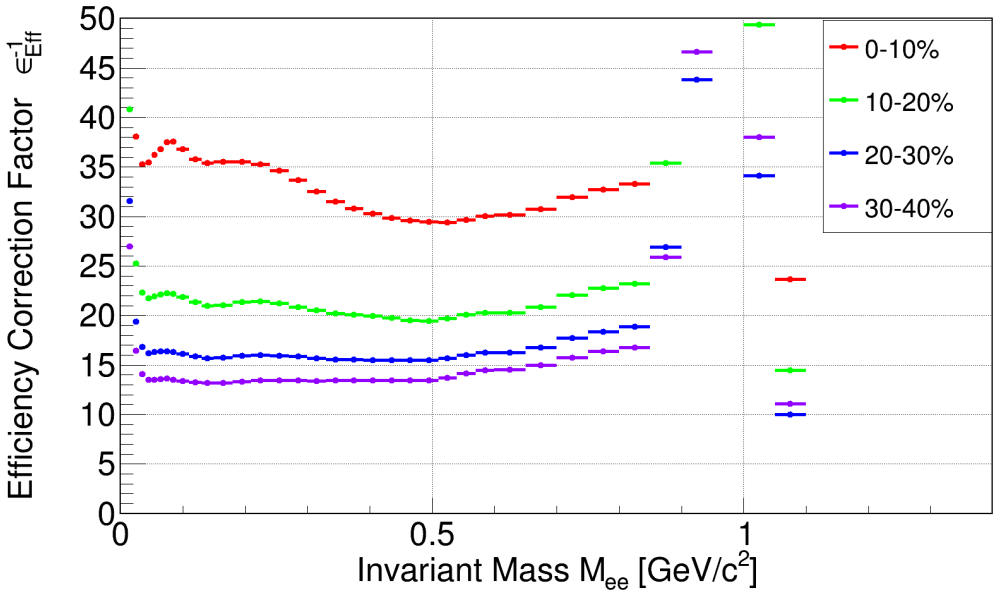

Figure 6.2: Efficiency Corrections for centrality classes between 0-40% centrality (Au+Au at $\sqrt{s_{NN}} = 2.42\ GeV$, HADES).

The simulations needed for the efficiency calculations are only available for these central events. Consequently, one has to resolve to extrapolating the data from figure 6.2. At first glance, one can already see how the differences in efficiency are decreasing for increasing centrality. To get a quantitative statement these differences are calculated and compared. For a better comparison the ratios of differences between centrality classes are calculated and those results are plotted in figure 6.3:

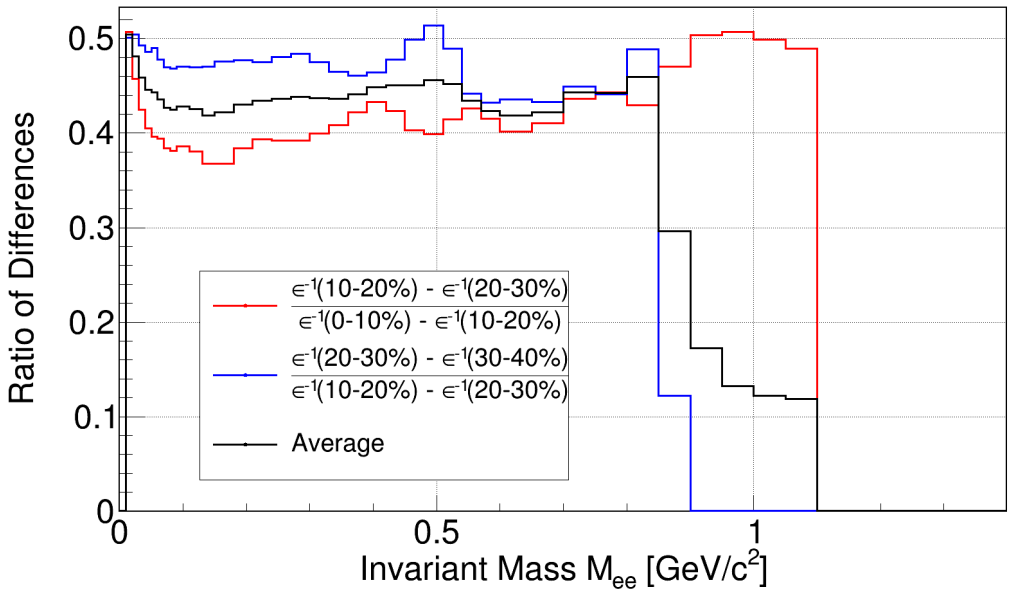

Figure 6.3: Ratio of differences in efficiency.

It can be seen that the differences of efficiency between two centrality classes change by a factor of around $0.4-0.5$. As these ratios are very similar it is assumed that they are the same for subsequent centrality classes. Consequently, the average Avg of these ratio is taken which shall be used to calculate the desired efficiency for the remaining centrality classes:

$$\epsilon_{Eff}(40-50\%)^{-1} = \epsilon_{Eff}(30-40\%)^{-1} - (\epsilon_{Eff}(30-40\%)^{-1} - \epsilon_{Eff}(20-30\%)^{-1}) \cdot Avg \quad (6.3)$$

$$\epsilon_{Eff}(50-60\%)^{-1} = \epsilon_{Eff}(40-50\%)^{-1} - (\epsilon_{Eff}(40-50\%)^{-1} - \epsilon_{Eff}(30-40\%)^{-1}) \cdot Avg \quad (6.4)$$

With these assumptions the final corrections used in this work can be presented:

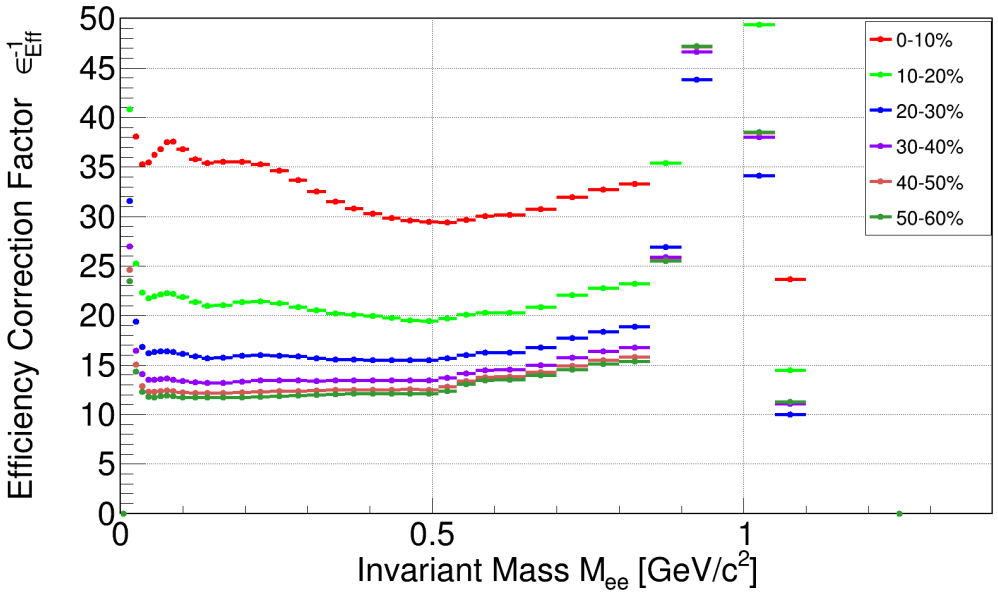

Figure 6.4: Efficiency Corrections for centrality classes between 0-60% centrality (Au+Au at $\sqrt{s_{NN}} = 2.42\ GeV$, HADES).

7 Evaluation of invariant mass spectra

With the processes described in the sections above one can create acceptance and efficiency corrected invariant mass spectra for dileptons. However, the resulting spectrum acts as an integral over the whole evolution of the fireball because the measured e^+e^- pairs are created in all stages of the collision. Since it is really only the hottest and densest phase that is interesting for this analysis, the spectra of freeze out source, namely the η-spectrum, and the spectra from the initial stage called the reference spectrum are subtracted from the Au+Au signals. In a first step one needs to normalize to number of π^0, only then the spectra can be compared and reference and η removed.

7.1 Normalisation to number of π^0

For normalisation every spectrum is divided by the total number of neutral pions N_{π^0}. To do this one first has to calculate the average number of pions per event for the different centrality classes. For central events this can be done by assuming $N_{\pi^0} \approx \frac{1}{2}(N_{\pi^+}N_{\pi^-})$ [10]. For peripheral events N_{π^+} and N_{π^-} have not been analyzed yet, which is why an extrapolation has been carried out. It is assumed that the behavior of the average number of pions $\langle N_{\pi^0}\rangle$ per event over the average number of participants $\langle A_{part}\rangle$ is as follows:

$$\langle N_{\pi^0}\rangle \propto \langle A_{part}\rangle^{\alpha} \tag{7.1}$$

With $\langle A_{part}\rangle$ known from table 3.1 and $\langle N_{\pi^0}\rangle$ known for 0-40% centrality from previous analysis [1], a fit has been carried out using Eq. 7.1:

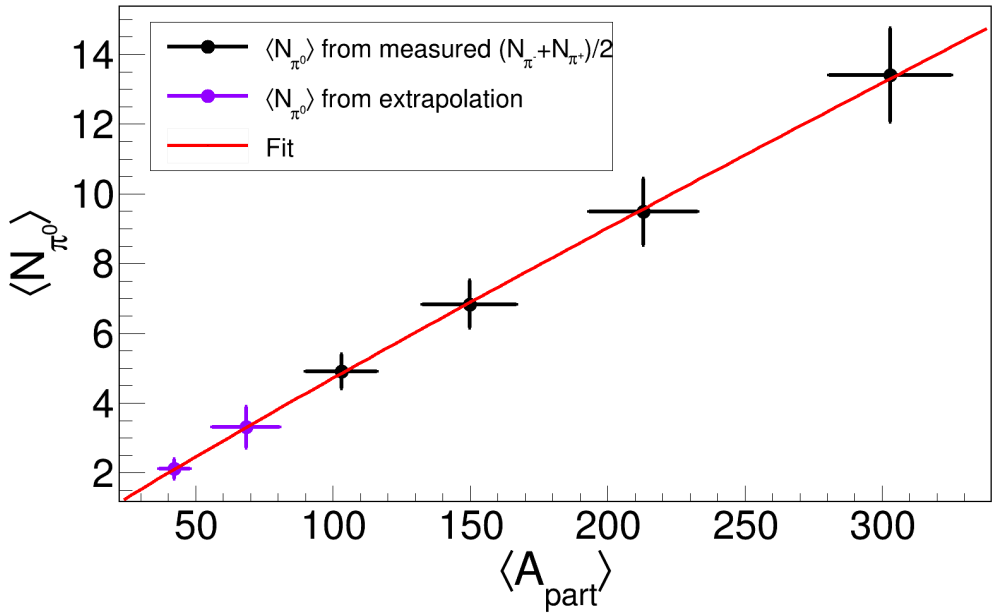

Figure 7.1: $\langle N_{\pi^0}\rangle$ over $\langle A_{part}\rangle$ from HADES for Au+Au at $\sqrt{s_{NN}} = 2.42\ GeV$.

The fit gives $\alpha = 0.94 \pm 0.17$ and the determined $\langle N_{\pi^0}\rangle$ are summarized in the following table:

Table 7.1: Number of pions per event for different centrality classes from HADES for Au+Au at $\sqrt{s_{NN}} = 2.42\ GeV$.

Centrality[%]	$\langle N_{\pi^0} \rangle$	$\Delta\langle N_{\pi^0} \rangle$
0-10	13.4	1.34
10-20	9.48	0.095
20-30	6.83	0.69
30-40	4.9	0.49
40-50	3.3	0.6
50-60	2.1	0.29

The error $\Delta\langle N_{\pi^0} \rangle$ was calculated using $\Delta\langle A_{part} \rangle$ and Gauss propagation of error. The total number of pions N_{π^0} used for normalisation is now the product of the average number per event times the number of events in this centrality class. The former can be taken from figure 3.2.

7.2 Isolation of excess pairs

In a next step the η- and reference-spectrum are to be subtracted from the Au+Au signal.

Looking at the η-spectrum first. Its shape has been calculated using simulations and its multiplicity is known for events between 0-40% centrality. In order to get the spectrum for peripheral collisions a power law, analogous to Eq. 7.1, is assumed. From [13] it is known that α lies in between $\alpha = 0.8$ for $2A\ GeV$ and $\alpha = 1.2$ for $1A\ GeV$. The energies for the Au+Au collisions are at $1.23A\ GeV$. With this knowledge it is assumed that the η-spectrum scales linear with A_{part}, meaning $\alpha = 1$. As one can see in figure 7.2, the contributions of the spectrum are smaller compared to the reference which is why this assumption should be sufficient for the purposes of this work.

The reference spectrum is known from elementary collisions at the same energy, namely np and pp experiments. As mentioned in section 1.2.3 the first chance collisions are characterized by such single NN-interactions. Therefore, the remaining pairs after subtraction of NN-collisions and η-spectrum are the excess pairs and indicate directly the change of yield in Au+Au collisions over elementary collisions. The advantage of this procedure is being able to directly compare excess yields from different collisions system in respect to elementary collisions.

In the following figure the Au+Au signal as well as the NN-reference and η-spectrum are plotted for comparison. For this every spectrum is efficiency corrected and normalized to number of neutral pions. However, since all spectra are taken from the same detector it does not matter whether the isolation of excess pairs is done before or after acceptance correction. In this case the spectra are not acceptance corrected.

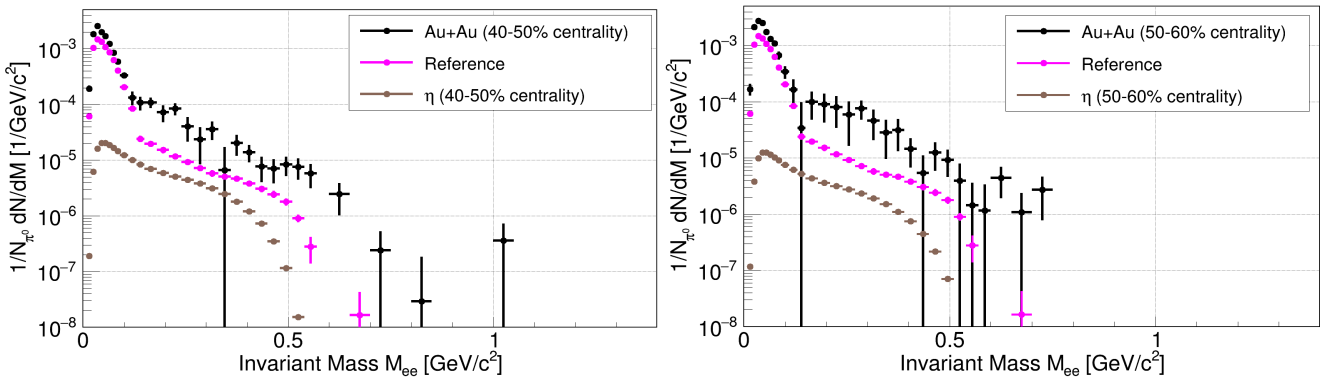

(a) 40-50% centrality **(b)** 50-60% centrality

Figure 7.2: Au+Au, Reference and η spectrum in comparison ($\sqrt{s_{NN}} = 2.42\ GeV$, HADES).

7.3 Systematic errors and final invariant mass spectra

After efficiency and acceptance correction, normalisation to the number of pions N_{π^0} as well as subtraction of reference and η-spectrum the final invariant mass distributions can be presented. Before this can be done however, it is important to discuss systematic error sources.

Since the data acquisition as well as the analysis process is separated into a multitude of steps there are many factors that could lead to a systematic error. For the purposes of this work the most dominant ones are taken into account and listed in the following:

- **Normalisation to number of pions:** From table 7.1 the systematic errors for the $\langle N_{\pi^0} \rangle$ are known and consequent systematic errors can be calculated accordingly.
- **Acceptance correction:** For the acceptance correction a systematic error of 10% is assumed.
- **Efficiency correction:** For the efficiency correction a systematic error of 10% is assumed. In addition, one has to take into account the systematic uncertainties stemming from the extrapolation. Hence, for 40-50% and 50-60% centrality a additional systematic error of 20% is estimated.
- **Reference spectrum:** For the reference spectrum systematic errors have been calculated in earlier works and their impact on the leftover Au+Au signal systematic uncertainty can be calculated accordingly.
- **Combinatorial Background:** The systematic errors for the combinatorial background are dependent on the Background-to-Signal ratio B/S. From [1] it is assumed that relative systematic error can be calculated with $B/S \cdot 0.02$.

All these errors are assumed to be independent from each other, such that the final error is given as the square root of their sum of squares. With this in mind the final spectra can be presented.

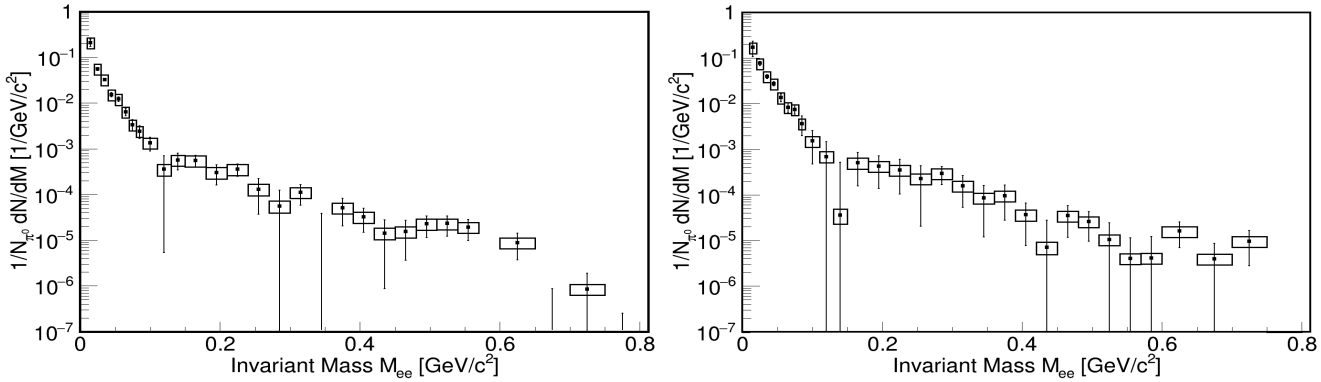

(a) 40-50% centrality **(b)** 50-60% centrality

Figure 7.3: Peripheral Au+Au invariant mass spectrum from HADES in work at $\sqrt{s_{NN}} = 2.42\ GeV$. Statistical errors are represented by bars and systematic errors represented by boxes.

Since they will be used in the following section, the invariant mass spectra for central events shall also be shown:

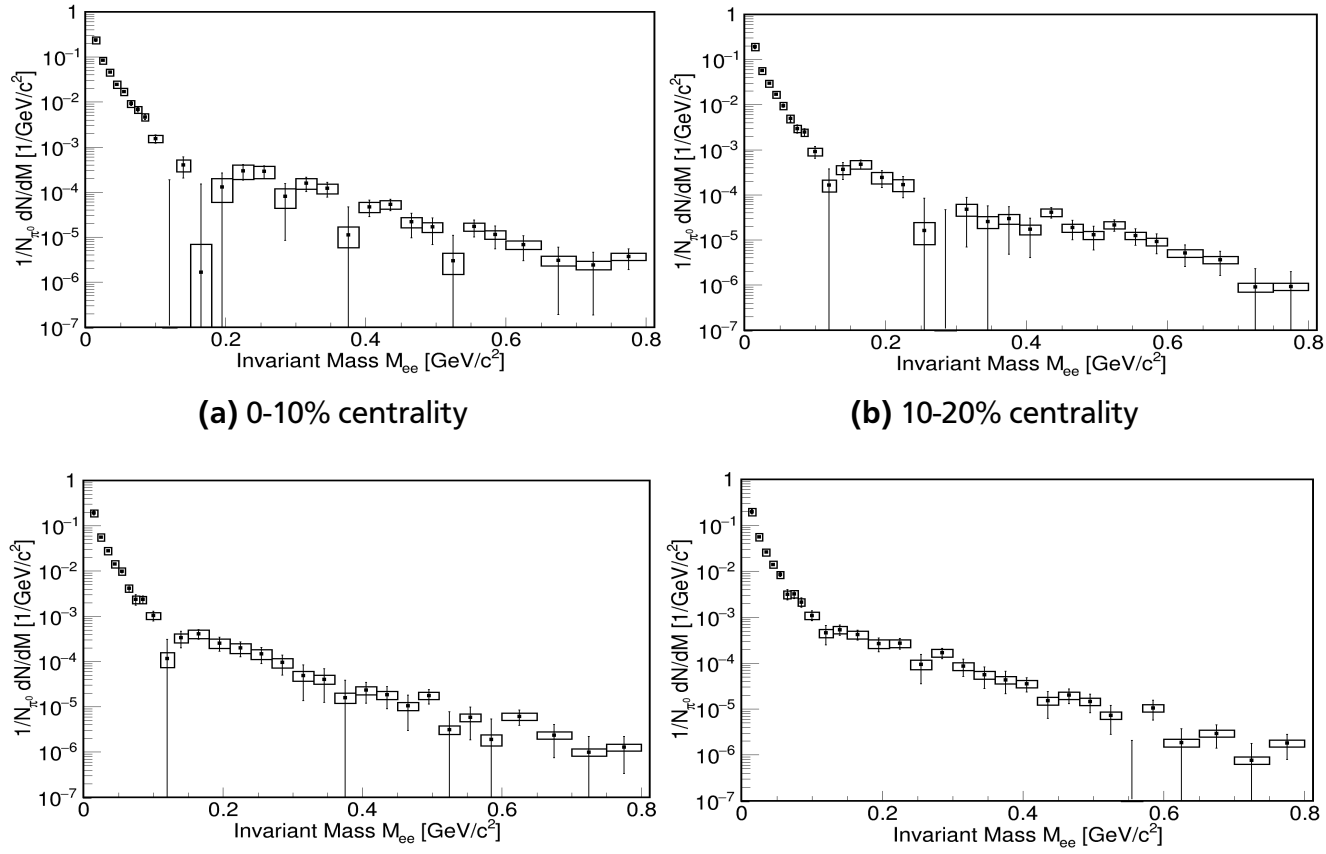

(a) 0-10% centrality **(b)** 10-20% centrality

(c) 20-30% centrality **(d)** 30-40% centrality

Figure 7.4: Central Au+Au invariant mass spectrum from HADES in work at $\sqrt{s_{NN}} = 2.42\ GeV$. Statistical errors are represented by bars and systematic erros represented by boxes.

7.4 Excess yield and temperature as a function of $\langle A_{part} \rangle$

In a final step properties from the fireball shall be extracted from the efficiency corrected, normalized, η and reference isolated, and acceptance corrected invariant mass spectra.

For one the integral of the pair spectrum gives the total excess yield. This is done for the six investigated centrality classes and can be plotted over the number of nucleons participating in the collision $\langle A_{part} \rangle$. It is assumed that the excess yield is proportional to $\propto \langle A_{part} \rangle^{\alpha}$. The region for the integral is chosen to be $0.3 - 0.7 GeV/c^2$ because the particularly interesting ρ-Meson supposedly has the largest contribution in this region.

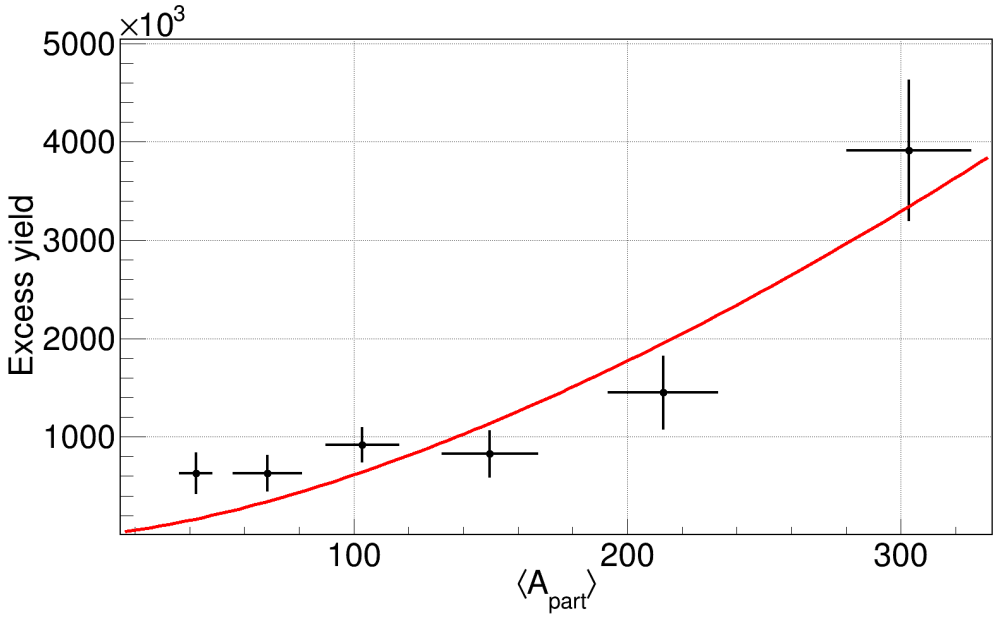

Figure 7.5: Excess yield over $\langle A_{part} \rangle$ from HADES for Au+Au at $\sqrt{s_{NN}} = 2.42\ GeV$. The data points are marked in black and the red curve represents the fit to determine α .

The fit gives: $\alpha = 1.53 \pm 0.36$. Previous analysis for 0-40% centrality has determined $\alpha_{previous} = 1.44 \pm 0.17$ [10]. Hence, the determined dependence of the excess yield over A_{part} is in agreement with previous results. However, it can also be noted that the determined α has a large relative error of roughly 24% and looking at figure 7.5 one can see that the data points are not aligned well with the fit.

Furthermore, the dilepton invariant mass distribution allows for a temperature determination of the fireball. More precisely, this is done by fitting the slope of the spectrum using a Boltzman-fit:

$$\frac{dN}{dM} \propto M^{3/2} \exp(-M/T) \tag{7.2}$$

This formula acts as an approximation for invariant masses above the π^0 mass range since the slope is largely influenced by thermal radiation after this point. With this in mind the fit range

has been chosen to be $0.2 - 0.8\ GeV/c^2$. Fitting in higher mass regions was neglected as not all centrality classes have measured a signal above $0.8\ GeV/c^2$ and the fit range should be the same for all cases.

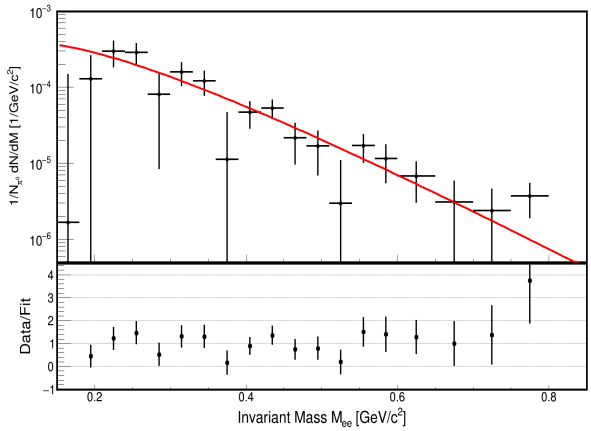

(a) 0-10% centrality

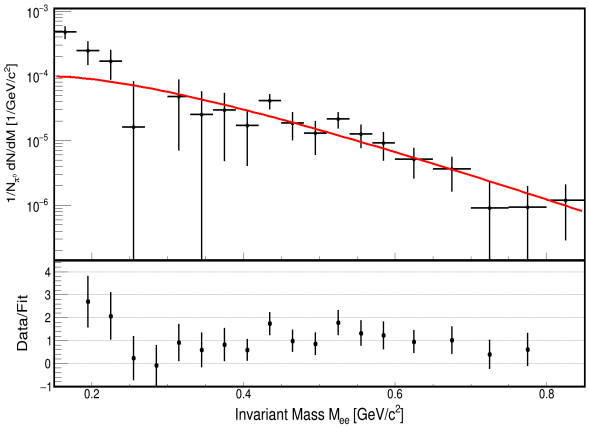

(b) 10-20% centrality

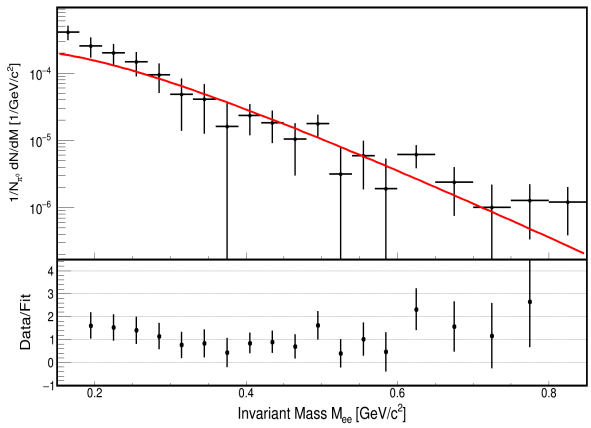

(c) 20-30% centrality

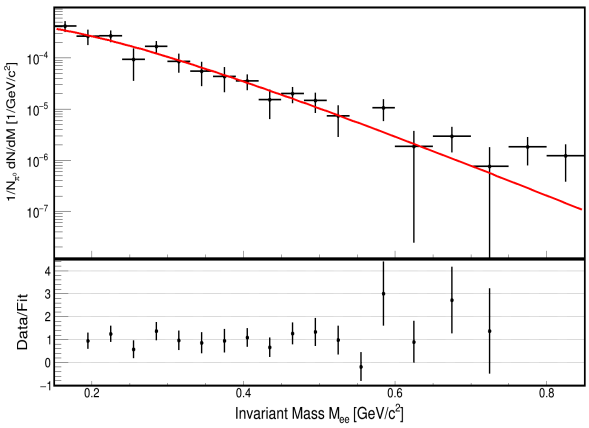

(d) 30-40% centrality

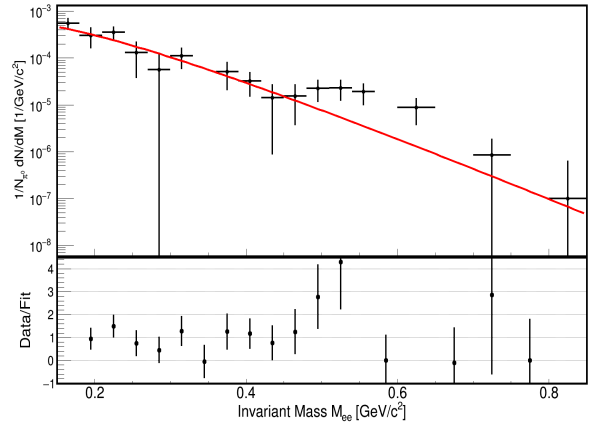

(e) 40-50% centrality

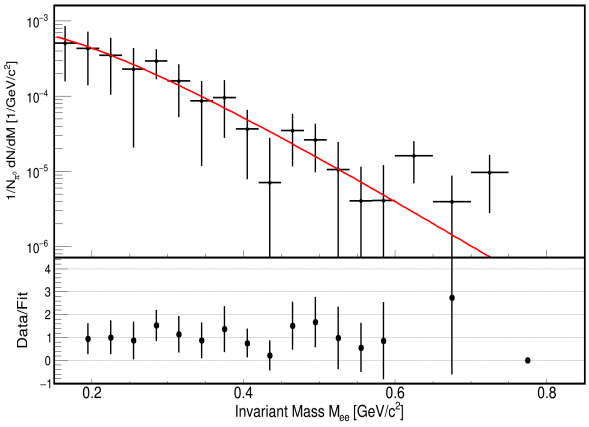

(f) 50-60% centrality

Figure 7.6: Temperature determination from dilepton spectra slopes (Au+Au at $\sqrt{s_{NN}} = 2.42\ GeV$, HADES). The black points are the data points and the red line represents the fit. Below the ratio of the two has been calculated and plotted.

Doing such a fit for every centrality class gives a temperature T each. In the following the results are plotted over $\langle A_{part} \rangle$:

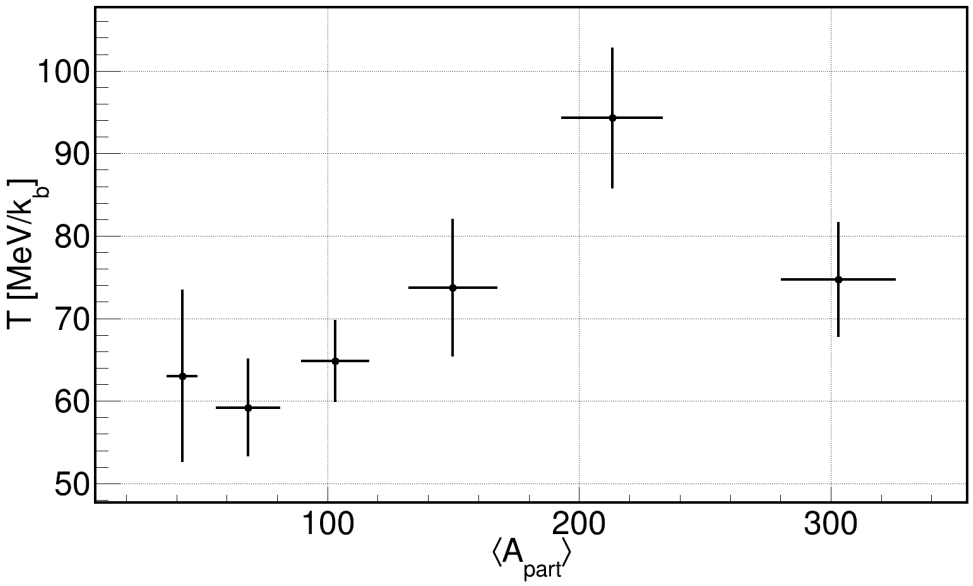

Figure 7.7: Fireball temperature over $\langle A_{part} \rangle$ from HADES for Au+Au at $\sqrt{s_{NN}} = 2.42\ GeV$. The temperature errors result from the fit.

After the centrality class 10-20% a a downtrend is visible but comes to halt for the final data point at 50-60% centrality. In addition for 0-10% centrality the temperature is unreasonably low with $T = 74.7 \pm 6.8\ MeV/k_b$ compared to 10-20% centrality with $T = 94.3 \pm 8.4\ MeV/k_b$. This indicates the resulting temperatures are to be handled with caution and a further inspection should be done first before coming to conclusions. The issues can be seen in figure 7.6 when looking at the fit-to-data ratios. Ideally it should be very close to one, however, it can be noticed how the ratios scatter from this desired value and the fit is not aligned properly with the data points. This is the case for all centralities. Previous analysis has shown, e.g. [1], that the slopes should fit the Boltzman distribution much better. Consequently these temperatures serve as a first result and more work is to be put into these temperature determination in the future.

8 Conclusion and outlook

In a first step of the analysis, all events were taken from the data summary tape and went through an event selection process, in order to gain a suitable sample of events. In this context, particular attention was paid to the physics triggers which lead to a necessary distinction between PT2 and PT3 events. Assuming an equal number of events over all centrality classes a new PT2 scaling with value 6 has been identified. Then the all particle candidates were scanned for leptons. More precisely, electrons and positrons were identified and selected using a multivariate analysis. In addition, a close pair cut was introduced which aims to reduce combinatorial background. The identified leptons were then assigned to pairs and an invariant mass distribution with all possible pair combinations was created. By subtracting the combinatorial background the actual signal, measured in the experiment, was received. The calculation of the CB was done using a combination of the same event and event-mixing method. Afterwards the signal was corrected for efficiency, whereas the efficiency for the peripheral events was extrapolated from the efficiency of the central events. The corrected signals were normalized to the number of π^0 such that reference and η-spectrum could be removed from the Au+Au signal. In a final step the leftover signal was corrected for acceptance and systematic errors were estimated.

Therefore, the first goal of reconstructing e^+e^- pairs for peripheral events, using the experimental data of Au+Au collision at $\sqrt{s} = 2.42\ GeV$, has been accomplished. In a follow up analysis the excess yield and temperature were extracted from the invariant mass spectra and plotted over the number of participants $\langle A_{part} \rangle$. The excess yield was found to scale with $\alpha = 1.53 \pm 0.36$ which is in agreement with results from earlier works.

However, for the temperature no clear trend was found and it is believed these calculations should be investigated further. In fact, even the excess yield do not align properly with the fit.

For these reasons, it would be interesting to build on the basis laid by this work and try to improve these results in the future. Possible reasons for the inconsistencies and ideas for improvement could, among other things, involve the following:

- **Efficiency Corrections for peripheral events using simulations:** In order to decrease systematic errors and minimize the risk of overlooking effects which could only effect peripheral events, it would be advantageous to also use simulations to calculate the efficiency in these centralities.
- **PT Weighting:** After the analysis was concluded, it was found that the number of PT2 events stored was changed during the experiment. This is the reason for the uneven distribution of number of events over centrality classes as seen in figure 3.1. Now the analysis could be repeated using the actual weights instead of relying on an average.
- **Averaging without close pair cut:** Experience at HADES has shown that calculating the average of one signal with and one signal without a close pair cut seems to smooth out the dilepton mass distribution. This in turn, might allow for better temperature determination.
- **Combinatorial Background** One factor that hugely influences the results is the method which is used to calculate the combinatorial background. Even using a different region for event-mixing normalisation has a noticeable effect in the properties extracted from

the signal. In addition, the combination of how much of the combinatorial background is described with the event-mixing or Same Event method is a topic of discussion. Hence, a thorough investigation on how to properly described the combinatorial background is elementary for the data analysis.

Bibliography

[1] Szymon Harabasz. *Reconstruction of virtual photons from Au+Au collisions at 1.23 GeV/u*. Darmstadt 2017.

[2] Jaroslav Bielcik. *Dilepton spectroscopy with HADES*. Darmstadt 2014.

[3] Patrick Seilheim. *Reconstruction of the low-mass dielectron signal in 1.23A GeV Au+Au collisions*. Frankfurt 2017.

[4] Claudia Behnke. *Reconstruction of π^0 and η Mesons via Conversion in 197 Au+ 197 Au at 1.23 GeV/u with the HADES Spectrometer*. Frankfurt 2016.

[5] David J. Thompson, *Space Detectors for Gamma Rays (100 MeV — 100 GeV): from EGRET to Fermi LAT*. Astroparticle Physics Laboratory, NASA Goddard Space Flight Center, Greenbelt, Maryland USA 2015

[6] `https://www.gsi.de/en/researchaccelerators/research_an_overview/hades_experiment/configuration_of_the_hades_experiment.htm` - accessed 01.07.2018.

[7] `https://www-zeuthen.desy.de/~kolanosk/astro0607/skripte/cosmics03.pdf` - accessed 01.07.2018.

[8] Bodgan Povh, Klaus Rith, Christoph Scholz, Frank Zetsche, Werner Rodejohann - Particles and Nuclei - An Introduction the the Physical Concepts - Seventh Edition - Springer Verlag 2015

[9] `https://hades-wiki.gsi.de/foswiki/bin/view/Homepages/Dielectrons` - accessed 01.07.2018

[10] J. Adamczewski-Musch et al. [HADES collaboration]. *Dielectron radiation from baryon-rich medium.* 2018

[11] Patrick Seilheim. *Dielektronenrekonstruktion in Au+Au Kollisionen bei 1.25 Gev/u (Simulation)*. Frankfurt 2011.

[12] J. Adamczewski-Musch et al. [HADES collaboration]. *Centrality determination of Au + Au collisions at 1.23A GeV*. 2018 with HADES

[13] R. Averbeck, R. Holzmann, et al.,Phys.Rev. C67 (2003) 024903

[14] L.G. Landsberg. *Electromagnetic Decays of light mesons.* Institute for High Energy Physics, Serpukhov, U.S.S.R., April 1985

[15] J. Pietraszko et al., *"Radiation damage in single crystal CVD diamond material investigated with a high current relativistic 197Au beam," Nuclear Instruments and Methods in Physics Research Section A: Accelerators, Spectrometers, Detectors and Associated Equipment* Volume 763, (2014). `http://www.sciencedirect.com/science/article/pii/S0168900214007013.`

[16] P Sellheim and HADES Collaboration 2015 J. Phys.: Conf. Ser. 599 012027. `http://iopscience.iop.org/article/10.1088/1742-6596/599/1/012027/pdf`

[17] G. Agakichiev R. et al. [HADES Collaboration]. *The high-acceptance dielectron spectrometer HADES*. 2009

[18] T. Galatyuk [HADES Collaboration], PoS INPC 2016 (2017) 354.

[19] P.M.Hohler and R.Rapp, *Is ρ-Meson Melting Compatible with Chiral Restoration?*, Phys. Lett. B 731 (2014) 103.